EXPERIMENTAL INVESTIGATION OF A CHARRING ABLATIVE MATERIAL EXPOSED TO COMBINED CONVECTIVE AND RADIATIVE HEATING IN OXIDIZING AND NONOXIDIZING ENVIRONMENTS

By John H. Lundell, Roy M. Wakefield, and Jerold W. Jones
Research Scientists
NASA, Ames Research Center, Moffett Field, California

Introduction

Entry into planetary atmospheres can involve both convective and radiative heating. In addition, if the atmosphere contains oxygen-bearing species, heating due to surface and ablation vapor combustion can occur. A number of experimental investigations of the performance of charring materials under convective heating in both reactive and inert gas streams have been conducted. Relatively little work has been done, however, on the performance of these materials under combined convective and radiative heating. Accordingly, a systematic investigation was conducted to evaluate the effects of the magnitude and relative proportions of combined convective and radiative heating on the effectiveness of a charring material in providing protection against entry heating. To evaluate the effectiveness, it is necessary to determine the interactions between the material ablation products and the external heating environment. These interactions are the blockage of convective heating by the ablation vapors, gas-phase combustion, and surface combustion. Tests to evaluate the ablation rates and the interactions were performed in a vacuum with radiative heating only, and in air and nitrogen streams with convective heating only, and combined convective and radiative heating. The tests were performed under steady-state heating rates. This paper presents, analyzes, and discusses the results of the tests and describes and applies a method for utilizing the results to predict the behavior of the charring material under conditions other than those of the present tests.

Experimental Equipment and Models

Facility

All tests were conducted in the Ames Entry Heating Simulator which is illustrated in Fig. 1 and described in reference 1. The facility consists of separate convective and radiative heating systems which can be operated either simultaneously or independently. The convective heating system is a wind tunnel with an arc-heated supersonic stream. A detailed description of the arc heater is given in reference 2. The radiative heating system consists of a carbon-arc radiation source and two ellipsoidal mirrors. Radiation from the arc is collected by one mirror, reflected into a converging-diverging beam, and then focused on the model by the other mirror. The beam enters the test chamber through a quartz window in the downstream end of the test chamber. Located at the window is a movable shutter which is used to control the duration of the radiative heat flux. A rotating chopper, also located near the window, periodically interrupts the beam to separate the surface emitted and reflected radiation to allow the measurement of the model surface temperature. The level of the applied radiative heating is controlled by placing wire-mesh screens in the beam.

Ablation Models

The ablation models were machined from phenolic nylon, which was a 50-50 mixture by weight of powdered phenolic and nylon resins, and had a density of 75 lb/ft^3. Molding and curing procedures were in accordance with the methods developed at Langley Research Center. The model (Fig. 2(a)) is a 0.75-inch-diameter hemisphere-cylinder with a 0.31-inch-diameter core. The outer shroud was undercut to reduce heat transfer between the core and shroud.

Instrumentation

The instrumentation employed in the present tests consisted of devices and systems to measure the following: (1) mass-flow rate of the test gas, and pressures in the arc-heater reservoir and test chamber; (2) radiative and cold-wall convective heating rates; (3) model surface pressure; (4) model surface temperature; and (5) ablation specimen mass, length, and internal interface locations.

The mass-flow rate of the test gas and the arc-heater reservoir pressure were determined with a system comprised of a calibrated venturi meter and precision Bourdon-type gages. All pressure gages were photographed at one-eighth second intervals throughout every run in order to indicate any variations in pressure during a run. Test chamber ambient pressure was measured prior to each run with a McLeod gage.

The radiative and cold-wall convective heating rates and the model surface pressure were measured with instrumented nonablating models that had the same shape and were located in the same position as those for the ablation models. The same heat-transfer model was used for determining the cold-wall convective rate and the applied radiative rate. It was a transient-type calorimeter (described in ref. 1) and had a copper slug of the same diameter as the ablation model core. A thermocouple was embedded in the rear of the copper slug to measure its temperature-time history. The heating rate was determined from the rate of change of the slug temperature. To measure the radiative heating rate, the calorimeter was blackened with camphor soot to produce a high surface absorptance. The pressure probe was made of copper and had a single 1/16-inch-diameter orifice leading from the stagnation point to tubing connected to a pressure transducer. The electrical signals from the calorimeter and pressure transducer were recorded on an oscillograph.

A monochromatic pyrometer, similar to one of the units used in the dual-band pyrometer described in reference 1, was used to measure the model surface temperature. The optical bandpass of the pyrometer was centered at approximately 0.84 micron and was 0.2 micron wide. The surface temperature was measured in the brief interval during which the radiation was interrupted by the rotating chopper.

NATIONAL AERONAUTICS AND SPACE ADMINISTRATION
AMES RESEARCH CENTER, MOFFETT FIELD, CALIFORNIA

A variety of instruments were used in performing measurements on the ablation specimens. An analytical balance was used to determine the mass of the specimens; a dial gage, mounted in a special fixture, was used to measure the length of the specimens; and a toolmakers microscope was used to measure the location of an interface between two zones in the ablated specimens.

Description of Tests and Measurements

Test Conditions and Procedures

Tests were performed with convective heating only and with combined convective and radiative heating in both air and nitrogen streams, and with only radiative heating in a vacuum. The ranges of the nominal test conditions are shown below, and the actual values are listed in table I:

RANGES OF NOMINAL TEST CONDITIONS

Test gas	Δh_{app}, $\frac{Btu}{lb}$	$\dot{q}_{c_{hw}}$ $\frac{Btu}{ft^2\text{-sec}}$	$\alpha\dot{q}_r$, $\frac{Btu}{ft^2\text{-sec}}$	$\frac{\alpha\dot{q}_r}{\dot{q}_{c_{hw}}}$	p_s, atm
Air	1000-3000	100-200	0-400	$0, \frac{1}{2}, 1, 2$	0.04-.16
Nitrogen	1100-5000	100-300	0-250	$\frac{1}{2}, 1$	.04-.16
Vacuum	---	---	100-500	---	---

For each test condition, initial calibration runs were made to establish the selected values of total enthalpy, pressure, cold-wall convective heating rate and radiative heating rate. Both the convective and radiative rates were constant throughout each run. Maximum run duration varied with test conditions and was imposed by either of two factors: the temperature rise limit of the heat-sink-type arc heater, or a significant reduction in the radiative heating rate resulting from deposition of ablation products on the window at the end of the test chamber. At each condition, ablation models were tested for a series of durations to determine the time variation of the ablation measurements. Additional calibration runs were made between some of the ablation runs and after the series of runs at each test condition.

Environmental Measurements

Significant environmental parameters in this investigation were total enthalpy, stagnation-point pressure, and the convective and radiative heating rates. Total enthalpy was evaluated by the equilibrium sonic-flow method described in reference 3. Enthalpy of the air stream was determined from the pressure rise versus enthalpy plot of reference 3; and the enthalpy of the nitrogen stream was determined from the nitrogen curves of reference 4. Separate runs were made to measure stagnation-point pressure over the complete ranges of total enthalpy and arc-reservoir pressure. Separate runs were also made to measure the cold-wall convective heating rate and the radiative heating rate at each test condition. The hot-wall convective heating rates were determined from the measured cold-wall rates.

Ablation Measurements

Ablation measurements consisted in weighing and measuring the model core before and after each run. The post-run condition of the specimen is illustrated in Fig. 2(b), a photograph of a sectioned model. It is apparent that the specimen consists of three distinct zones: a char zone, a pyrolysis zone, and the virgin material. The boundaries of these zones with respect to the initial surface position of the unablated model are denoted by X_s, X_c, and X_p.

A quantity defined as pyrolysis mass loss (m_p) was determined from the weight measurements. Pyrolysis mass loss is the difference between the pre-run core mass and the post-run core mass with the char cap removed (see "Pyrolysis Rate" for discussion of the significance of pyrolysis mass loss). The char cap was removed intact and weighed separately. It always separated in a clean break, and the surface of the core after removal had much the same appearance as the char surface. The material remaining on the core was very thin, however, and not electrically conductive, whereas both the front and rear surfaces of the char cap were conductive (resistance of 15 ohms or less).

From the length measurements, the recessions of the various interfaces were determined. Surface recession (X_s) is the difference between the pre-run and the post-run core length before removal of the char cap. Recession of the char interface (X_c) is the difference between the pre-run and the post-run core length with the char cap removed. Recession of the pyrolysis interface (X_p) was determined by cutting the model core in half and measuring the thickness of the pyrolysis zone with a microscope. The thickness was added to the char interface recession to obtain the pyrolysis interface recession.

Experimental Results

The time variation of the ablation measurements and the surface temperature for a typical test condition are illustrated in Fig. 3. After a transient period, the time variation of the ablation measurements became linear and the surface temperature attained an essentially steady-state value. (In the worst case, the rate of temperature rise at the end of the longest run did not exceed 10° R per second.) The slopes of the linear portion of the ablation measurement curves were used to determine the pyrolysis rate, surface velocity, char interface velocity, and pyrolysis interface velocity. These quantities and the final surface temperatures for all test conditions are listed in table I.

From the surface and internal interface velocities presented in Fig. 3 and table I, it is apparent that $V_p > V_c > V_s$ at any given test condition; hence, the pyrolysis and char zones increased at constant rates. These conditions occurred in all of the present tests. It is not known whether they would have existed for runs longer than those of the present tests (maximum run duration varied from 6 to 29 seconds).

From measurements of the surface temperature at two different wavelengths, the surface emittance was estimated to be 0.85. The char surface was assumed to be a grey body so the absorptance was also 0.85.

Analysis and Discussion of Results

The test results have been analyzed to determine the effects of both the magnitude and the

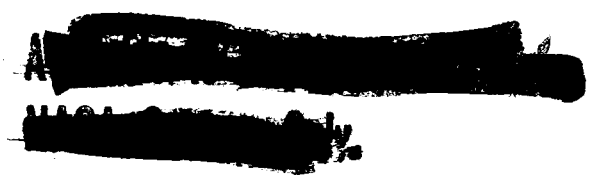

NATIONAL AERONAUTICS AND SPACE ADMINISTRATION
AMES RESEARCH CENTER, MOFFETT FIELD, CALIFORNIA

relative proportions of the convective and radiative components of the total applied heating rate on the ablation behavior of phenolic nylon. Based on results of the analysis a method has been developed for predicting ablation behavior under conditions other than those of the present tests. In the present section, the method is developed by first relating the ablation behavior to surface temperature and then relating surface temperature to the applied heating rate.

Ablation Behavior

The ablation of phenolic nylon can be characterized by several ablation rates. An important one is the pyrolysis rate ($\dot{m}_p$) which is the rate of production of the end products of pyrolysis, namely, carbonaceous char and ablation vapors. Another is the char removal rate ($\dot{m}_{cr}$). The pyrolysis rate will be discussed first.

Pyrolysis rate.- The pyrolysis rate is the sum of the vapor-production and the char-production rates. This fact can be demonstrated by considering the manner in which $\dot{m}_p$ is determined. Pyrolysis mass loss is the difference in mass between the unablated model core and the post-run core with the char cap removed. In terms of the interface location (see Fig. 2(b))

$$m_p = \rho_m X_c + (\rho_m - \rho_p)(X_p - X_c) \qquad (1)$$

where ρ_m is the density of the virgin material and ρ_p is the mean density in the pyrolysis zone. The term $\rho_m X_c$ is the mass (per unit area) of the material which has been completely degraded to char and vapors, and the term $(\rho_m - \rho_p)(X_p - X_c)$ is the mass of vapor produced in the pyrolysis zone. Pyrolysis rate is the time derivative of the pyrolysis mass loss; thus

$$\dot{m}_p = \rho_m V_c + (\rho_m - \rho_p)(V_p - V_c) \qquad (2)$$

Equation (2) can be rearranged as follows

$$\dot{m}_p = \underbrace{(\rho_m - \rho_c)V_c}_{\substack{\text{Rate of production of} \\ \text{vapors in completely} \\ \text{degraded material}}} + \underbrace{(\rho_m - \rho_p)(V_p - V_c)}_{\substack{\text{Rate of production of} \\ \text{vapors in partially} \\ \text{degraded material}}} + \underbrace{\rho_c V_c}_{\substack{\text{Char-production} \\ \text{rate}}} \qquad (3)$$

The first two terms are the vapor-production rate ($\dot{m}_{vp}$) and the third term is the char-production rate ($\dot{m}_{cp}$). Thus

$$\dot{m}_p = \dot{m}_{vp} + \dot{m}_{cp} \qquad (4)$$

A correlation of all measured values of pyrolysis rate with surface temperature is shown in Fig. 4. The correlation includes results from tests with radiation only, convection only, and convection and radiation combined in both air and nitrogen streams. (The various symbols are listed in table I.) The fact that all the results correlate on a common curve demonstrates that $\dot{m}_p$ is a function solely of the surface temperature, and the correlation is unaffected by (1) the mode of heat transfer, (2) the occurrence of combustion, and (3) the surface pressure.

The two components of the pyrolysis rate were determined in the following manner. The char-production rate was evaluated from the measurements of ρ_c and V_c. The mean-char density was determined for each ablation model, and the results indicate it is a function of surface temperature. It increases from about 20 lb/ft^3 at 4000° R to about 26 lb/ft^3 at 5600° R. Values of the char interface velocity for each test condition are listed in table I. With these results, the char-production rate was determined, and then the vapor-production rate was determined from Eq. (4). The char- and vapor-production rates are plotted against surface temperature in Fig. 5. Data for all test conditions are included in the figure; from the results, it is concluded that both the char- and vapor-production rates are functions solely of the surface temperature. These correlations are unaffected by the mode of heat transfer, the occurrence of combustion, and surface pressure. In a later section, the vapor-production rate will be shown to be particularly important in the correlation of both convective blockage and gas-phase combustion effects.

In any application of the present results, it is important to know the rate at which the pyrolysis zone advances into the virgin material. From the correlation of $\dot{m}_p$ and V_p with surface temperature, it can be shown that for these tests,

$$V_p = \frac{\dot{m}_p}{0.85\ \rho_m} = 0.016\ \dot{m}_p \qquad (5)$$

Char-removal rate.- Char-removal rate is related to the surface recession velocity (V_s) by the equation

$$\dot{m}_{cr} = \rho_c V_s \qquad (6)$$

Surface recession velocity has been determined for all test conditions and is listed in table I. These values, together with the measured char density, have been used to determine $\dot{m}_{cr}$, and the results are plotted as a function of surface temperature and pressure in Fig. 6.

Comparison of the results of tests with radiation only and in nitrogen shows that the nitrogen stream was inert. These results correlate on a common curve labeled "inert environment." The mechanisms responsible for the finite surface recession in the inert environment are not known. Because of the agreement between the nitrogen and radiation data, it is concluded that the mechanism is neither aerodynamic shear nor chemical reactions between the nitrogen and the char surface. One possible mechanism is shrinkage. The sharp increase in char-removal rate in heating by radiation only at a temperature of about 5550° R is attributed to sublimation of the char. Hence, 5550° R is taken to be the sublimation temperature of phenolic nylon char corresponding to the pressure at which these tests were performed ($100 < p_s < 300$ microns).

A consistent family of pressure-dependent curves is faired through the air data and indicate that in an air stream the char-removal rate increases with both increasing surface temperature and pressure. The increment between any of the air curves and the inert environment curve ($\Delta\dot{m}_{cr}$) is attributed to surface combustion. Because of differences in the environment at the char surface between the radiation only and air-flow cases, it is not known whether sublimation effects are present in the air data.

NATIONAL AERONAUTICS AND SPACE ADMINISTRATION
AMES RESEARCH CENTER, MOFFETT FIELD, CALIFORNIA

The results shown in Fig. 6 can be analyzed to determine the nature of the surface combustion reaction. Such reactions are usually classified as diffusion controlled, reaction-rate controlled, or transitional between diffusion and rate controlled. In the diffusion-controlled regime, the oxidation process is controlled by the amount of oxygen which diffuses through the boundary layer to the surface. In this case, the mass-loss rate due to surface combustion is given by an equation of the form[5,6]

$$\Delta\dot{m}_{cr} = C\sqrt{\frac{p_s}{R_n}} \qquad (7)$$

where R_n is the nose radius. Equation (7) indicates that in the diffusion-controlled regime the reaction depends on the surface pressure and the nose radius and is independent of the temperature. In the rate-controlled regime there is sufficient oxygen at the surface for the oxidation process to be controlled by the chemical-reaction rate. In this case, the mass-loss rate due to surface combustion is given by an equation of the Arrhenius form[7,8]

$$\Delta\dot{m}_{cr} = K_o(p_{o_s})^n e^{-E/RT_s} \qquad (8)$$

The form of Eq. (8) indicates that in the rate-controlled regime, the surface combustion reaction depends upon surface temperature and the partial pressure of oxygen at the surface and is independent of nose radius. The char-removal rate due to surface combustion shown in Fig. 6 exhibits a strong dependence on temperature, thus suggesting that in the present tests, the surface combustion was reaction-rate controlled.

On the basis of this suggestion, a correlation of the values of $\Delta\dot{m}_{cr}$ was attempted. It was found that the values could be correlated with the surface temperature and the square root of surface pressure as shown in Fig. 7. The fact that this correlation is based on $(p_s)^{1/2}$ rather than on $(p_{o_s})^n$ suggests a relationship between the two pressures. Such a relationship has not been established because of uncertainties in the effects of convective blockage and gas-phase combustion on the oxygen partial pressure at the surface.

The correlation shown in Fig. 7 may not be applicable to other heating conditions if:

(1) The surface pressure is outside the range of the present tests;

(2) The nose radius differs from that of the present tests - for bodies of larger nose radius, the surface combustion may be diffusion controlled;

(3) Convective blockage and gas-phase combustion effects are different from those of the present tests - these effects tend to reduce the diffusion of oxygen to the surface.

Relationship Between Surface Temperature and Applied Heating Rate

The correlations just presented demonstrate that the ablation behavior of phenolic nylon is a function of the surface temperature. Thus if surface temperature can be determined for any given applied heating condition, the ablation behavior can be determined. In this section the surface heat balance is discussed and the applied heat ($\dot{q}_{app}$) is related to the net heat that reaches the surface ($\dot{q}_n$). The relationship involves terms representing the effects of convective blockage, surface combustion, and gas-phase combustion. The experimental results are used to evaluate the blockage and combustion effects and to relate $\dot{q}_n$ to surface temperature.

Surface heat balance.- The various terms in the surface heat balance are presented in sketch (a).

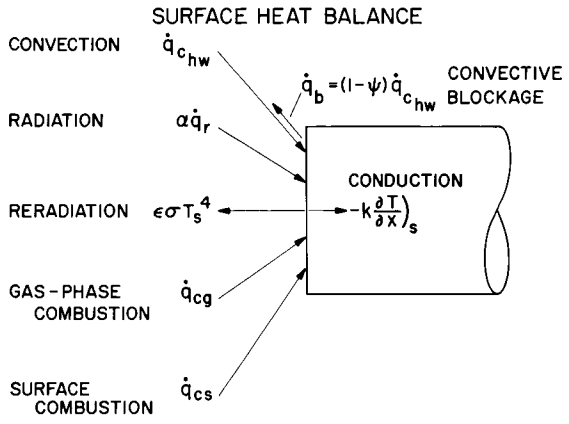

Sketch (a)

The equation for the surface heat balance can be written as follows:

$$\dot{q}_{c_{hw}} - \dot{q}_b + \alpha\dot{q}_r + \dot{q}_{cg} + \dot{q}_{cs} - \epsilon\sigma T_s^4 = -k\left(\frac{\partial T}{\partial x}\right)_s \qquad (9)$$

Define $\dot{q}_{app} = \dot{q}_{c_{hw}} + \alpha\dot{q}_r$ as the applied heating rate, and $\dot{q}_n$ as the net heat reaching the surface. Then,

$$\dot{q}_n = \dot{q}_{app} - \dot{q}_b + \dot{q}_{cg} + \dot{q}_{cs} = \epsilon\sigma T_s^4 - k\left(\frac{\partial T}{\partial x}\right)_s \qquad (10)$$

With this equation, $\dot{q}_n$ can be determined for a given $\dot{q}_{app}$ if the heating rates due to convective blockage, gas-phase combustion, and surface combustion are known.

The individual terms in Eq. (10) were evaluated by tests in different environments. The $\dot{q}_n$ term was determined from results of the radiation only tests, $\dot{q}_b$ was determined from results of the tests in a nitrogen stream, and the combustion terms were determined from results of the tests in an air stream.

Net heating rate.- In the case of a radiation only environment, the equation for $\dot{q}_n$ reduces to

$$\dot{q}_n = \dot{q}_{app} = \alpha\dot{q}_r = \epsilon\sigma T_s^4 - k\left(\frac{\partial T}{\partial x}\right)_s \qquad (11)$$

The results of tests in the radiation only environment are listed in table I and shown in Fig. 8 where $\dot{q}_n = \alpha q_r$ is plotted against surface temperature. The onset of sublimation is readily apparent since $\dot{q}_n$ becomes essentially independent of temperature at about 5550° R. At higher

NATIONAL AERONAUTICS AND SPACE ADMINISTRATION
AMES RESEARCH CENTER, MOFFETT FIELD, CALIFORNIA

pressures, the sublimation temperature will increase and the $\dot{q}_n$ curve will not flatten off until a higher value of $\dot{q}_n$ is reached. (Note that when sublimation occurs, an additional term representing the heat absorbed in the sublimation process must be added to Eq. (11).) The dashed line in Fig. 8 represents the energy reradiated from the surface when the char is assumed to be a grey-body radiator with an emittance of 0.85. At any given surface temperature, the horizontal spacing between the vertical axis and the dashed curve represents the portion of $\dot{q}_n$ which is reradiated from the surface, and the spacing between the two curves represents the portion of $\dot{q}_n$ which is conducted into the material. Note that for temperatures below the onset of sublimation, conduction is about 23 percent of $\dot{q}_n$.

It is of interest to determine the amount of conducted heat absorbed per pound of pyrolyzed material. The quantity $-k[\partial T/\partial x)_s]/\dot{m}_p$ increased from 1395 Btu/lb at 4000° R to 1790 Btu/lb at 5400° R in the present tests. These values are 50 to 90 percent larger than the corresponding value for Teflon.

Convective blockage.- In the case of a nitrogen stream which was essentially inert in the present tests, the equation for $\dot{q}_n$ reduces to

$$\dot{q}_n = \dot{q}_{app} - \dot{q}_b \tag{12}$$

where $\dot{q}_b = (1 - \psi)\dot{q}_{c_{hw}}$. The factor ψ is the ratio of the convective heating rate to an ablating surface to the convective heating rate to a nonablating surface at the same temperature. This factor can be determined from Eq. (12) for each test condition in nitrogen since all the other terms are known.

Results of the nitrogen tests are listed in table II and shown in Fig. 9 which is a plot of ψ against the mass transfer parameter B. The solid line is a fairing through the results of the present tests, and the dashed line is a prediction computed by the method of reference 9 for a mean molecular weight of the ejected vapors of about 15. The two data points at the highest value of B are for combined convective and radiative heating. Bars are attached to these points to indicate the uncertainty in ψ for these tests due to changes in the level of radiative heating caused by deposition of ablation vapors on the window at the end of the test chamber.

The trend of the present results agrees reasonably with the predicted curve at higher values of B, but departs significantly at lower values of B. In fact, the measured values indicate increases rather than the predicted decreases in heat transfer. Similar results at low values of B have been reported in forced mass-transfer studies. Barber[10] obtained values of ψ in excess of 1.0 for injection of hydrogen, helium, and nitrogen into air at the stagnation point of an axisymmetric body. Pappas and Okuno[11] obtained similar results for injection of helium into a laminar air boundary layer along the surface of a cone.

Surface combustion.- The surface combustion heating rate, $\dot{q}_{cs}$, was determined from the results of the surface recession measurements by the equation

$$\dot{q}_{cs} = \Delta\dot{m}_{cr}H_{rc} \tag{13}$$

where H_{rc} is the heat of reaction of the surface oxidation process, and $\Delta\dot{m}_{cr}$ is the increment of char removal due to surface combustion. It was assumed that all the heat released in the surface combustion reaction adds directly to $\dot{q}_n$ (Eq. (10)).

The heat of reaction was computed on the assumption that the oxygen in the air stream was an equilibrium mixture of the atomic and molecular species at the surface pressure and temperature. The heats of reaction of atomic and molecular oxygen with carbon were obtained from thermo-chemical properties.[12] The end product of the surface combustion was assumed to be carbon monoxide. The heat of reaction ranged from 4350 to 7300 Btu/lb char for surface temperature and pressure of 4170° R and 0.045 atm and 5390° R and 0.072 atm, respectively.

Gas-phase combustion.- In evaluating the gas-phase combustion heating rate, $\dot{q}_{cg}$, occurring during the tests in air, all the terms in Eq. (10) must be considered. Thus,

$$\dot{q}_n = \dot{q}_{app} - \dot{q}_b + \dot{q}_{cs} + \dot{q}_{cg} \tag{14}$$

The term $\dot{q}_{cg}$ can be evaluated from this equation since all the other terms are known. The correlation shown in Fig. 9 is employed to evaluate the convective heat blockage. To determine the mass-transfer parameter B, in an air stream, the CO released in the surface reaction is included as a component of the vapors injected into the boundary layer. The rate of CO production is 2.33 $\Delta\dot{m}_{cr}$ so that the mass-transfer parameter becomes

$$B = (\dot{m}_{vp} + 2.33\ \Delta\dot{m}_{cr})\ \frac{\Delta h_{app}}{\dot{q}_{c_{hw}}} \tag{15}$$

In order to develop a correlation for $\dot{q}_{cg}$, use was made of the concept that the effect of combustion reactions can be treated as an increase in the enthalpy potential. (This concept has been used elsewhere.[13-15]) Thus the total convective heat input to the surface is assumed to be of the form

$$\psi\dot{q}_{c_{hw}} + \dot{q}_{cg} \sim (\Delta h_{app} + \Delta h_{cg}) \tag{16}$$

where Δh_{cg} is the enthalpy increment associated with the combustion reactions. Evaluation of this enthalpy increment depends upon whether there is sufficient oxygen to react with all the vapors. For an oxygen-rich mixture, the following relation is used,

$$\Delta h_{cg} = \frac{\dot{m}_{vp}H_{rv}}{\rho_e v_e} \tag{17}$$

where $\rho_e v_e$ is the mass flux of air at the boundary-layer edge, and H_{rv} is the mean heat of reaction per pound of vapor. In a fuel-rich mixture, Δh_{cg} is not proportional to $\dot{m}_{vp}$, but is equal to the value for a stoichiometric mixture; that is,

$$\Delta h_{cg} = \frac{H_{rv}}{k} \tag{18}$$

where k is the mass of air per unit mass of vapors required for a stoichiometric mixture. In the present tests, the occurrence of surface combustion shows that all the oxygen was not consumed by vapor combustion; that is, oxygen-rich combustion occurred.

NATIONAL AERONAUTICS AND SPACE ADMINISTRATION
AMES RESEARCH CENTER, MOFFETT FIELD, CALIFORNIA

Since the gas-phase combustion heating is treated as a convective input, it is of interest to relate the combustion heating to the net convective heating that would reach the surface in the absence of combustion. From Eqs. (16) and (17)

$$\frac{\dot{q}_{cg}}{\psi \dot{q}_{c_{hw}}} = \frac{\Delta h_{cg}}{\Delta h_{app}} = H_{rv} \frac{\dot{m}_{vp}}{\rho_e v_e \Delta h_{app}} \qquad (19)$$

An expression for the mass flux of air at the edge of the boundary layer, $\rho_e v_e$, can be developed from the work of Howe.[16] The result is

$$\rho_e v_e = 0.0414\, f_e \sqrt{\left(\frac{p_s}{R_n}\right)\left(\frac{T_e}{T_e + 203}\right)}\, Z_e^{-1/4} \qquad (20)$$

where f_e and T_e are the stream function and temperature, respectively, at the edge of the boundary layer, and Z_e is the compressibility factor. With the expression for $\rho_e v_e$ from Eq. (20), the final form of Eq. (19) becomes

$$\frac{\dot{q}_{cg}}{\psi \dot{q}_{c_{hw}}} = \frac{H_{rv}}{f_e}\left[\frac{\dot{m}_{vp}}{0.0414\sqrt{\left(\frac{p_s}{R_n}\right)\left(\frac{T_e}{T_e + 203}\right)}\, Z_e^{-1/4} \Delta h_{app}}\right] = \frac{H_{rv}}{f_e} G \qquad (21)$$

This equation suggests the quantities that must be considered in correlating the data on gas-phase combustion heating. Those quantities appearing within the brackets are either known from the measurements or can be directly evaluated. It is difficult, however, to evaluate H_{rv} and f_e. For H_{rv}, the specific chemical reactions must be known; such knowledge is not presently available. Values of f as a function of the dimensionless distance from the surface are given in reference 17 for the case of mass transfer, but it is difficult to identify the boundary-layer edge distances appropriate to the test conditions. However, neither H_{rv} nor f_e need be evaluated for correlation purposes if they are essentially constant for the range of test conditions considered. It can be shown[17] that f_e was reasonably constant for the present test conditions. The constancy of H_{rv} cannot be established a priori; however, the assumption that it was essentially constant appears reasonable from a consideration of the probable combustion reactions.

The results for gas-phase combustion heating are correlated on the foregoing basis in Fig. 10. The random scatter about the mean fairing is no greater than might be expected considering that $\dot{q}_{cg}$ is the last term to be evaluated from the heat balance equation. From the correlation presented in Fig. 10, the following is concluded: (1) gas-phase combustion heating can be treated as a convective process; and (2) the mean heat of reaction of the gas-phase chemical reactions was relatively constant.

Effects of Magnitude and Relative Proportions of Applied Heat

With the correlations of the ablation behavior and the evaluations of the convective blockage and gas-phase and surface combustion, the ablation performance of phenolic nylon can be predicted for steady-state heating conditions other than those of the present tests. Also, the effects of the magnitude and the relative proportions of the convective and radiative components of the applied heating rate can be determined. The parameter chosen to describe the performance is the effective heat of ablation, which is defined as

$$H_{eff} = \frac{\dot{q}_{app}}{\dot{m}_p} = \frac{\dot{q}_{c_{hw}} + \alpha \dot{q}_r}{\dot{m}_p} \qquad (22)$$

Thus H_{eff} represents the amount of applied thermal energy accommodated per unit mass of material pyrolyzed. From Eq. (10) it is apparent that H_{eff} can be expressed as follows:

$$H_{eff} = \frac{\dot{q}_{app}}{\dot{m}_p} = \frac{1}{\dot{m}_p}\left[\dot{q}_b + \epsilon\sigma T_s^4 - k\left(\frac{\partial T}{\partial x}\right)_s - \dot{q}_{cg} - \dot{q}_{cs}\right] \qquad (23)$$

The applied heating is accommodated by convective blockage, reradiation from the surface or conduction into the material. Offsetting these accommodation mechanisms are the gas-phase and surface combustion heating effects.

The ablation performance is predicted by an iterative technique which can be described as follows: For given values of $\dot{q}_{c_{hw}}$, $\alpha\dot{q}_r/\dot{q}_{c_{hw}}$, R_n, and Δh_{app}:

(1) Assume a surface temperature and evaluate the convective blockage and combustion heating.

(2) Determine $\dot{q}_n$ from Eq. (10), and from Fig. 8, find surface temperature.

(3) Repeat until the final value of surface temperature agrees with the assumed value.

(4) With the final value of temperature, determine the pyrolysis rate from Fig. 4.

(5) Compute H_{eff} from Eq. (22).

This method has been applied to determine the effect of the magnitude and mode of heat transfer on the ablation performance of phenolic nylon for the following two series of heating conditions in an air stream:

	Series 1	Series 2
$\dot{q}_{c_{hw}}$, Btu/ft^{2}sec	400, 200, 133	200
$\alpha\dot{q}_r$, Btu/ft^{2}sec	0, 200, 267	0, 200, 400
$\alpha\dot{q}_r/\dot{q}_{c_{hw}}$	0, 1, 2	0, 1, 2
$\dot{q}_{app}$, Btu/ft^{2}sec	400	200, 400, 600
R_n, ft	0.0313 (3/8 in.)	0.0313
Δh_{app}, Btu/lb	3000 to 20,000	3000 to 20,000

The first series was selected to illustrate the effect of the relative proportion of the applied heat by keeping the magnitude of the applied heating ($\dot{q}_{app}$) constant and varying the proportions of radiation and convection ($\alpha\dot{q}_r/\dot{q}_{c_{hw}}$). The second series was selected to illustrate the interaction between the magnitude and relative proportions of the applied heat by keeping $\dot{q}_{c_{hw}}$ constant and adding various increments of radiation. A comparison of the two series illustrates the effect of magnitude of applied heating alone. Since $\dot{q}_{c_{hw}}$ and R_n are held constant in series 2, the stagnation-point

NATIONAL AERONAUTICS AND SPACE ADMINISTRATION
AMES RESEARCH CENTER, MOFFETT FIELD, CALIFORNIA

pressure decreases with increasing Δh_{app}. In series 1, R_n is held constant and $\dot{q}_{c_{hw}}$ is different for each value of $\alpha\dot{q}_r/\dot{q}_{c_{hw}}$; hence, the variation of pressure with Δh_{app} is different for each value of $\alpha\dot{q}_r/\dot{q}_{c_{hw}}$

In determining the effects of convective blockage, it was necessary to extrapolate the experimental ψ curve of Fig. 9 to higher values of B. For this purpose, the prediction computed by the method of reference 9 was extended beyond the range shown in Fig. 9. The resulting curve will approach an asymptotic value of $\psi = 0$ at a value of B of about 2. The effect of using a finite asymptote will be discussed.

The results of the calculations of H_{eff} for series 1 and 2 are plotted against Δh_{app} in Figs. 11(a) and (b), respectively. To illustrate the effects of the various heat accommodation mechanisms, the several components of H_{eff} are also plotted. From these results, it can be concluded that the most effective heat accommodation mechanisms are convective blockage and reradiation. Under high convection conditions, convective blockage is larger than reradiation; and under high radiation conditions, the opposite is true. Under all conditions, the heat accommodation by pyrolysis and storage (i.e., the conduction component) is small. It should be noted that under all conditions examined the heat added by both gas-phase and surface combustion is small and decreases with increasing Δh_{app}. The summation of the heat accommodation terms, less the combustion terms, increases with increasing Δh_{app}, causing H_{eff} to increase with increasing Δh_{app}.

The increase in H_{eff} continues until the heat accommodation by convective blockage reaches a maximum corresponding to a value of $\psi = 0$. When this occurs, all the applied convective heating is blocked, and all the components of H_{eff} become essentially constant. An asymptotic value of $\psi = 0$ may not be realistic. Test results for Teflon[1] indicate that ψ approaches a finite asymptote. Since test results at large values of B are lacking for phenolic nylon, the exact asymptotic value of ψ is unknown. However, the effect of a finite value can be illustrated if ψ is assumed to approach 0.1. For the condition $\dot{q}_{c_{hw}}$ = 200 Btu/ft^{2}sec, $\alpha\dot{q}_r$ = 200 Btu/ft^{2}sec, and Δh_{app} = 20,000 Btu/lb, H_{eff} = 11,200 Btu/lb for $\psi = 0$ and 9700 Btu/lb for $\psi = 0.1$.

The effect on H_{eff} of changing the relative proportions of convective to radiative heating at a constant magnitude of $\dot{q}_{app}$ is illustrated in Fig. 12(a). The curves illustrate that the variation of H_{eff} with Δh_{app} is not the same for different proportions of radiative to convective heating. At high enthalpy, H_{eff} is highest for convective heating, whereas at low enthalpy, the opposite is true.

Fig. 12(b) shows the changes in H_{eff} resulting from adding various increments of radiative heating to a given magnitude of convective heating. The trends with the proportion of radiative to convective heating are essentially the same as those shown in Fig. 12(a). By comparing the results in Figs. 12(a) and (b), one can determine the effect of the magnitude of applied heating. At a given value of $\alpha\dot{q}_r/\dot{q}_{c_{hw}}$, H_{eff} increases with increased $\dot{q}_{app}$ (compare curves for either $\alpha\dot{q}_r/\dot{q}_{c_{hw}}$ = 0 or 2).

Conclusions

From the results of the investigation of the ablation of phenolic nylon under the various heating conditions, the following conclusions are reached:

1. The ablation can be characterized by the mass rate of pyrolysis of the material, the end products of pyrolysis being vapors and a carbonaceous residue. The pyrolysis rate correlated solely on the basis of surface temperature, and thus at a given surface temperature, was independent of the mode of heating. Surface temperature itself was a function of both the magnitude and mode of heating.

2. The effective heat of ablation, defined as the applied heat accommodated per unit mass of material pyrolyzed, was dependent upon the heating conditions. The effectiveness increased with increasing total applied heating rate for constant proportions of radiative to convective heating. As the proportion of radiative heating was increased for a constant total heating rate, the effectiveness increased at low enthalpies, and decreased at high enthalpies.

3. For convective heating alone, and for combined convective and radiative heating, the dominant heat-accommodation mechanisms were the blockage of convective heating by the ablation vapors, and the reradiation of heat by the hot char surface. The heat absorbed in pyrolyzing the material was small for all conditions examined.

4. Two mechanisms involving the interaction of the ablation vapors with boundary-layer species, the blockage of convective heating and gas-phase combustion, could be correlated on the basis of theoretical considerations.

5. Char recession was found to increase with surface temperature for all heating conditions. Essentially identical results were obtained for radiative heating in a vacuum, and for various combinations of heating in a nitrogen stream. The reason for char recession under these conditions is not understood. Higher recession rates occurred in an air stream; the incremental rates were a function not only of surface temperature but also of pressure. The incremental recession in air is attributed to reaction-rate limited oxidation.

Nomenclature

B	mass transfer parameter, $(\dot{m}_{vp}\Delta h_{app}/\dot{q}_{c_{hw}})$
C	constant in Eq. (7)
E	activation energy, Btu/lb-mole
f	dimensionless stream function
G	defined by Eq. (21)
h_t	stream total enthalpy, Btu/lb
Δh_{app}	applied enthalpy potential, $(h_t - h_s)$, Btu/lb
Δh_{cg}	enthalpy potential due to gas-phase combustion, Btu/lb

NATIONAL AERONAUTICS AND SPACE ADMINISTRATION
AMES RESEARCH CENTER, MOFFETT FIELD, CALIFORNIA

H_{eff}	effective heat of ablation, Btu/lb
H_{rc}	heat of reaction of surface material, Btu/lb
H_{rv}	heat of reaction of vapors, Btu/lb
k	thermal conductivity
k	mass flux of air per unit mass of vapors for stoichiometric mixture
K_o	frequency factor, $lb/ft^2(atm)^n sec$
m_p	pyrolysis mass loss per unit area, lb/ft^2
$\dot{m}_p$	pyrolysis rate, $lb/ft^2 sec$
$\dot{m}_{cp}$	char-production rate, $lb/ft^2 sec$
$\dot{m}_{cr}$	char-removal rate, $lb/ft^2 sec$
$\dot{m}_{vp}$	vapor-production rate, $lb/ft^2 sec$
n	pressure exponent
p	pressure, atm
$\dot{q}_{app}$	applied heating rate, $Btu/ft^2 sec$
$\dot{q}_b$	convective heating rate blocked by mass transfer, $Btu/ft^2 sec$
$\dot{q}_{c_{hw}}$	hot-wall convective heating rate, $Btu/ft^2 sec$
$\dot{q}_{cg}$	gas-phase combustion heating rate, $Btu/ft^2 sec$
$\dot{q}_{cs}$	surface combustion heating rate, $Btu/ft^2 sec$
$\dot{q}_n$	net heating rate, $Btu/ft^2 sec$
$\dot{q}_r$	radiative heating rate, $Btu/ft^2 sec$
R	universal gas constant, Btu/lb-mole ^oR
R_n	body nose radius, ft
T	temperature, ^oR
V	interface velocity, ft/sec
v	stream velocity component normal to body, ft/sec
X	distance along body center line from original position of unablated surface, ft
x	distance normal to body surface, ft
Z	compressibility factor
α	surface absorptance
Δ	increment of change
ϵ	surface emittance
ρ	density, lb/ft^3
σ	Stefan-Boltzmann constant
ψ	heat blockage factor $\left(1 - \frac{\dot{q}_b}{\dot{q}_{c_{hw}}}\right)$

Subscripts

c	char
e	boundary-layer edge
m	virgin material
o	oxygen
p	pyrolysis
s	surface

References

1. Lundell, John H., Winovich, Warren, and Wakefield, Roy: Simulation of Convective and Radiative Entry Heating. Symposium on Hypervelocity Techniques, Denver, Colorado, March 20-21, 1962.

2. Shepard, C. E., and Winovich, W.: Electric-Arc Jets for Producing Gas Streams With Negligible Contamination. ASME Paper 61-WA-247.

3. Winovich, Warren.: On the Equilibrium Sonic-Flow Method for Evaluating Electric-Arc Air-Heater Performance. NASA TN D-2132, 1964.

4. Jorgensen, Leland H.: The Total Enthalpy of a One-Dimensional Nozzle Flow With Various Gases. NASA TN D-2233, 1964.

5. Scala, S. M.: The Ablation of Graphite in Dissociated Air. Pt. I Theory. IAS Paper 62-154.

6. Welsh, W. E., Jr., and Chung, P. M.: An Analysis of the Effect of Heterogeneous Reaction Kinetics on the Combustion of Graphite at the Stagnation Region of a Blunt Body in Hypersonic Flow. Rep. TDR-169(3230-12)TN6 Aerospace Corporation, El Segundo, Calif., Contract no. AF 04(695)-169, Feb. 1963.

7. Khitrin, L. N.: Physics of Combustion and Explosion. National Science Foundation, Wash., D. C., OTS 61-31205, 1962.

8. Glasstone, Samuel, Laidler, Keith, and Eyring, Henry: The Theory of Rate Processes. McGraw-Hill, New York, 1941.

9. Swann, R. T., and Pittman, C. M.: Numerical Analysis of the Transient Response of Advanced Thermal Protection Systems for Atmospheric Entry. NASA TN D-1370, 1962.

10. Barber, E. A.: An Experimental Investigation of Stagnation Point Injection. AIAA Paper 63-433.

11. Pappas, C., and Okuno, A.: Heat Transfer Measurements for Binary Gas Laminar Boundary Layer With High Rates of Injection. NASA TN D-2473, 1964.

12. JANAF Interim Thermochemical Tables. The Dow Chemical Co., Midland, Mich., Dec. 31, 1960.

13. Cohen, C. B., Bromberg, R., and Lipkis, R. P.: Boundary Layers With Chemical Reactions Due to Mass Addition. Jet Propulsion, vol. 28, no. 10, Oct. 1958, pp. 659-668.

14. Hartnett, J. P., and Eckert, E. R. G.: Mass Transfer Cooling With Combustion in a Laminar Boundary Layer. Proc. 1958 Heat Transfer and Fluid Mechanics Institute, Stanford University Press.

15. Lees, Lester: Convective Heat Transfer With Mass Addition and Chemical Reactions. Third AGARD Colloquium on Combustion and Propulsion, Pergamon Press, New York, 1958, pp. 451-498.

NATIONAL AERONAUTICS AND SPACE ADMINISTRATION
AMES RESEARCH CENTER, MOFFETT FIELD, CALIFORNIA

16. Howe, John T.: Shielding of Partially Reflecting Stagnation Surfaces Against Radiation by Transpiration of an Absorbing Gas. NASA TR R-95, 1961.

17. Emmons, H. W., and Leigh, D.: Tabulation of the Blasius Function With Blowing and Suction. Combustion Aerodynamics Lab. Interim Tech. Rep. 9, Div. of Applied Science, Harvard University, Nov. 1953.

NATIONAL AERONAUTICS AND SPACE ADMINISTRATION
AMES RESEARCH CENTER, MOFFETT FIELD, CALIFORNIA

TABLE I.- TEST CONDITIONS AND ABLATION MEASUREMENTS

Point no.	Symbol	Test gas	h_t, Btu/lb	p_s, atm	Δh_{app}, Btu/lb	$\dot{q}_{chw}$, $\frac{Btu}{ft^2 sec}$	$\alpha\dot{q}_r$, $\frac{Btu}{ft^2 sec}$	$\frac{\alpha\dot{q}}{\dot{q}_{chw}}$	T_s, ^oR	$\dot{m}_p$, $\frac{lb}{ft^2 sec}$	$\dot{m}_{vp}$, $\frac{lb}{ft^2 sec}$	$\dot{m}_{cp}$, $\frac{lb}{ft^2 sec}$	$\dot{m}_{cr}$, $\frac{lb}{ft^2 sec}$	V_s, ft/sec	V_c, ft/sec	V_p, ft/sec	Max. run time	No. of models
1	◇	Air	2420	0.160	1020	101	0	0	4560	0.0428	0.0318	0.0110	0.00764	0.000335	0.000483	0.000621	28	5
2	↓		2540	↓	1010	98	49	.50	4800	.0472	.0348	.0124	.00834	.000354	.000525	.000679	23	3
3			2690		970	97	98	1.01	5000	.0519	.0370	.0149	.00982	.000396	.000600	.000817	24	3
4			3100		1060	109	190	1.74	5400	.0611	.0420	.0191	.01202	.000466	.000742	.000965	24	3
5	○		3080	.045	1880	99	0	0	4170	.0270	.0191	.0079	.00424	.000197	.000367	.000479	29	5
6	↓		3330	↓	1880	102	47	.46	4410	.0363	.0273	.0090	.00475	.000212	.000400	.000494	24	4
7			3290		1790	97	88	.91	4690	.0361	.0256	.0105	.00538	.000230	.000450	.000552	24	3
8			3800		2030	107	205	1.92	5000	.0468	.0307	.0161	.00674	.000271	.000658	.000726	24	4
9	□		3310	.160	1810	176	0	0	4780	.0434	.0306	.0128	.00782	.000330	.000542	.000657	16	3
10	↓		3660	↓	1930	187	99	.53	5130	.0580	.0387	.0193	.00976	.000392	.000775	.000896	16	4
11			3750		1800	178	193	1.08	5360	.0632	.0411	.0221	.01116	.000433	.000858	.001021	12	5
12			4240		2100	207	348	1.67	5550	.0928	.0638	.0290	.01355	.000517	.001108	.001348	10	3
13	△		4490	.072	3040	193	0	0	4660	.0424	.0306	.0110	.00619	.000267	.000508	.000723	24	5
14	↓		4590	↓	2800	183	94	.51	5030	.0458	.0315	.0143	.00779	.000316	.000583	.000716	24	3
15			5010		2880	188	207	1.10	5390	.0618	.0426	.0192	.00899	.000347	.000742	.000955	16	3
16			5690		3140	215	385	1.79	5530	.0959	.0638	.0321	.01015	.000388	.001225	.001558	6	3
17	▱		3210	.16	1830	145	0	0	4520	.0417	.0317	.0100	.00700	.000310	.000442	.000692	20	3
18	↓	N_2	2170	.159	1140	110			3700	.0248	.0189	.0059	.00183	.000092	.000233	.000360	20	3
19			2470	.16	1310	116			4170	.0323	.0242	.0081	.00213	.000099	.000342	.000538	21	4
20			2920	.097	1720	131			4250	.0290	.0248	.0042	.00200	.000092	.000350	.000481	20	3
21			3950	.181	2640	234			4600	.0400	.0277	.0123	.00334	.000145	.000525	.000662	15	5
22			4900	.069	3570	281			4630	.0422	.0302	.0120	.00334	.000145	.000483	.000700	15	3
23			5360	.045	4160	232			4250	.0326	.0251	.0075	.00182	.000083	.000342	.000483	20	3
24			5390	↓	4010	221	132	.60	4860	.0519	.0338	.0181	.00338	.000142	.000758	.000937	12	2
25			5140		3680	207	244	.85	5050	.0552	.0376	.0176	.00357	.000145	.000717	.000783	8	2
26			6320	.072	5000	291	0	0	4600	.0419	.0321	.0098	.00334	.000145	.000525	.000700	8	2
27	▱	Vacuum	0	.0004	0	0	92	---	3460	.0174	.0132	.0042	.00170	.000096	.000167	.000279	22	4
28							168	---	4200	.0308	.0204	.0104	.00225	.000104	.000371	.000529	26	2
29							209	---	4430	.0323	.0241	.0082	.00246	.000110	.000367	.000479	23	3
30							246	---	4650	.0372	.0260	.0112	.00232	.000100	.000438	.000629	21	2
31							356	---	5100	.0465	.0334	.0131	.00272	.000110	.000533	.000639	20	5
32							374	---	5250	.0521	.0306	.0215	.00336	.000133	.000700	---	17	2
33							475	---	5450	.0611	.0384	.0227	.00445	.00017	.00093	.001080	11	4
34	↓		↓	↓	↓	↓	720	---	5550	.0608	.0413	.0195	.01230	.00047	.00075	---	10	3

NATIONAL AERONAUTICS AND SPACE ADMINISTRATION
AMES RESEARCH CENTER, MOFFETT FIELD, CALIFORNIA

TABLE II.- COMPONENTS OF SURFACE HEAT BALANCE

Point no.	$\epsilon\sigma T_s^4$, Btu/ft^{2}sec	$k\left(\frac{\partial T}{\partial x}\right)_s$, Btu/ft^{2}sec	$\dot{q}_n$, Btu/ft^{2}sec	$\dot{q}_{cs}$, Btu/ft^{2}sec	$\dot{q}_{cg}$, Btu/ft^{2}sec	B	Ψ	G, lb/Btu	$\dot{q}_{cg}/\dot{q}_{chw}$	$\frac{\Delta m_{cr}}{\sqrt{p_s}}$, lb(atm)$^{-1/2}$ft^{2}sec
1	173	57	230	23	127	0.421	0.777	0.000346	1.59	0.01225
2	218	57	275	27	128	.479	.724	.000352	1.855	.01375
3	257	68	325	32	126	.504	.645	.000425	1.91	.01570
4	349	101	450	44	144	.573	.614	.000442	2.18	.01920
5	124	40	164	10	81	.505	.735	.000218	1.11	.01034
6	155	47	202	11	84	.556	.647	.000312	1.40	.01132
7	199	52	251	13	90	.582	.658	.010307	1.525	.01270
8	257	67	324	18	54	.706	.471	.000325	1.018	.01566
9	214	68	272	24	111	.458	.712	.000191	.81	.01232
10	284	76	360	33	105	.551	.558	.000226	.875	.01537
11	338	100	438	39	91	.579	.470	.000258	.850	.01755
12	389	136	550	---	---	.814	.201	---	---	.02205
13	193	52	245	17	115	.595	.674	.000171	1.128	.01313
14	263	69	332	24	110	.627	.622	.000192	1.08	.01641
15	346	97	444	28	107	.732	.551	.000252	1.13	.01760
16	384	123	525	---	---	1.006	.158	---	---	.0203
17	172	48	220	22	104	.518	.690	.000195	1.11	.01146
18	77	38	115	0	0	.208	1.045	---	---	---
19	123	41	164	↓	↓	.283	1.422	---	---	---
20	134	41	175			.282	1.335	---	---	---
21	185	50	235			.315	1.00	---	---	---
22	189	51	240			.396	.854	---	---	---
23	134	41	175			.450	.754	---	---	---
24	229	61	290			.614	.754/.656	---	---	---
25	267	73	340			.670	.656/.232	---	---	---
26	185	50	235			.512	.808	---	---	---
27	60	37	97			---	---	---	---	0
28	128	40	168			---	---	---	---	↓
29	158	52	210			---	---	---	---	
30	192	54	246			---	---	---	---	
31	278	78	356			---	---	---	---	
32	312	88	400			---	---	---	---	
33	361	114	475			---	---	---	---	
34	389	331	720	↓	↓	---	---	---	---	↓

NATIONAL AERONAUTICS AND SPACE ADMINISTRATION
AMES RESEARCH CENTER, MOFFETT FIELD, CALIFORNIA

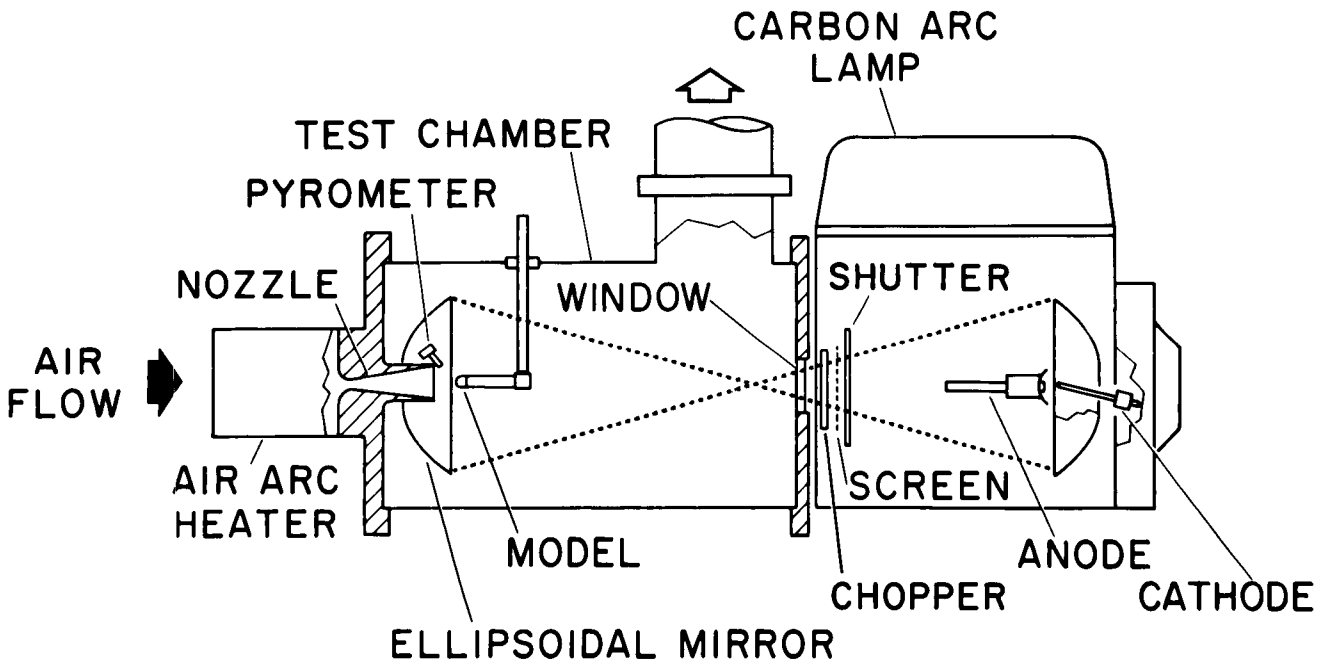

Fig. 1.- Ames entry heating simulator.

NATIONAL AERONAUTICS AND SPACE ADMINISTRATION
AMES RESEARCH CENTER, MOFFETT FIELD, CALIFORNIA

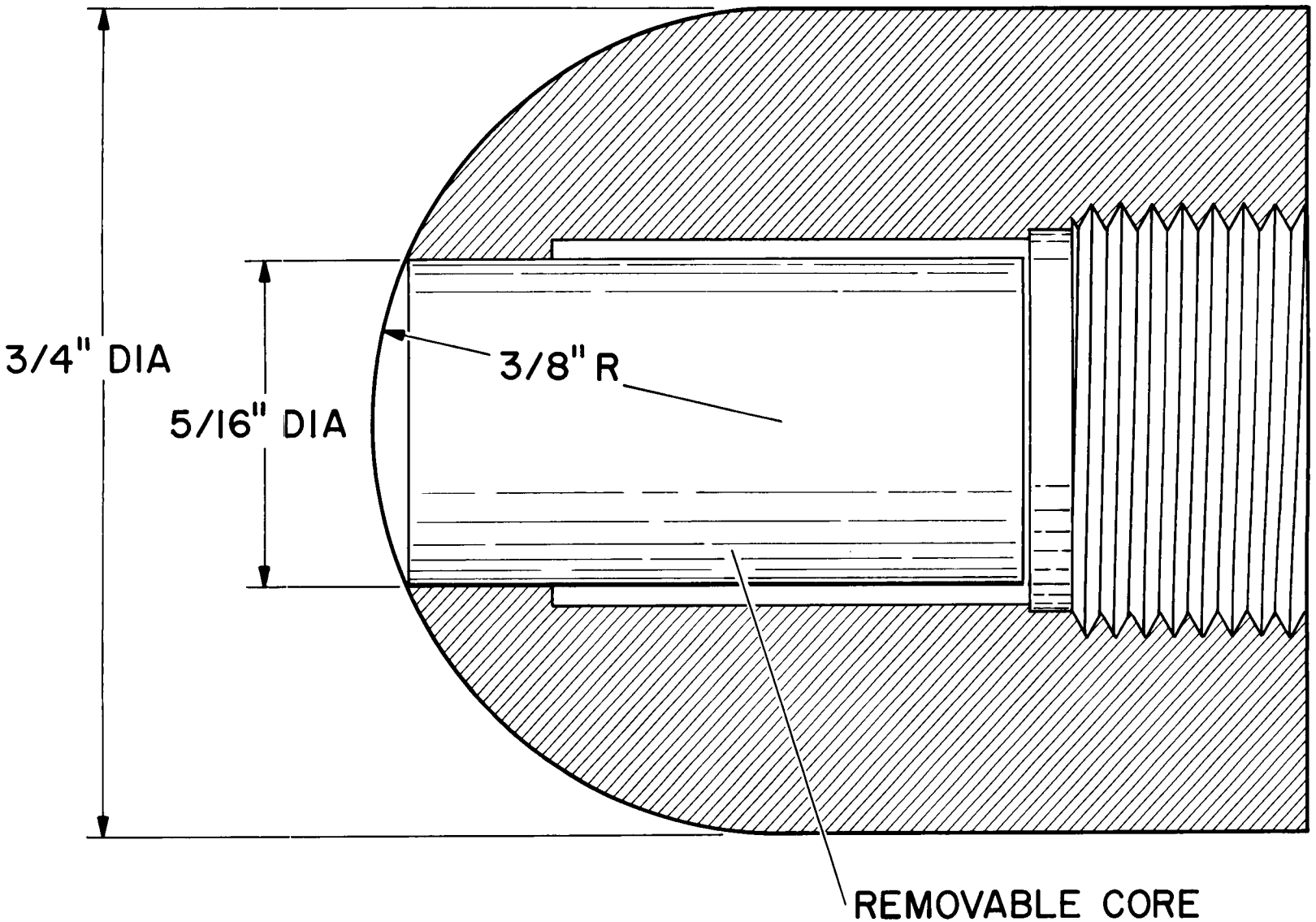

(a) Pre-run shape of model.

Fig. 2.- Ablation model.

NATIONAL AERONAUTICS AND SPACE ADMINISTRATION
AMES RESEARCH CENTER, MOFFETT FIELD, CALIFORNIA

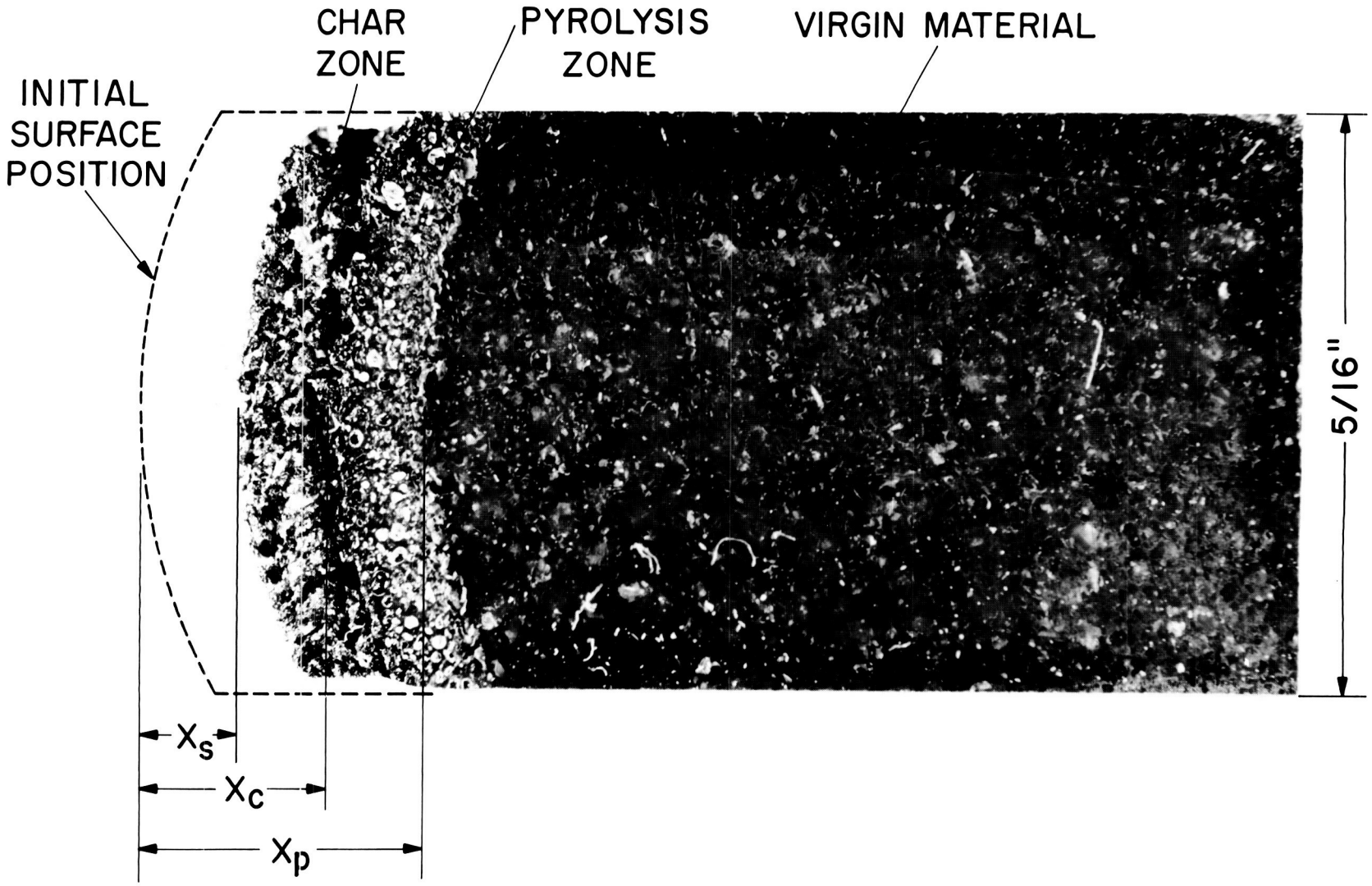

(b) Post-run condition of model core.

A-32879

Fig. 2.- Concluded.

NATIONAL AERONAUTICS AND SPACE ADMINISTRATION
AMES RESEARCH CENTER, MOFFETT FIELD, CALIFORNIA

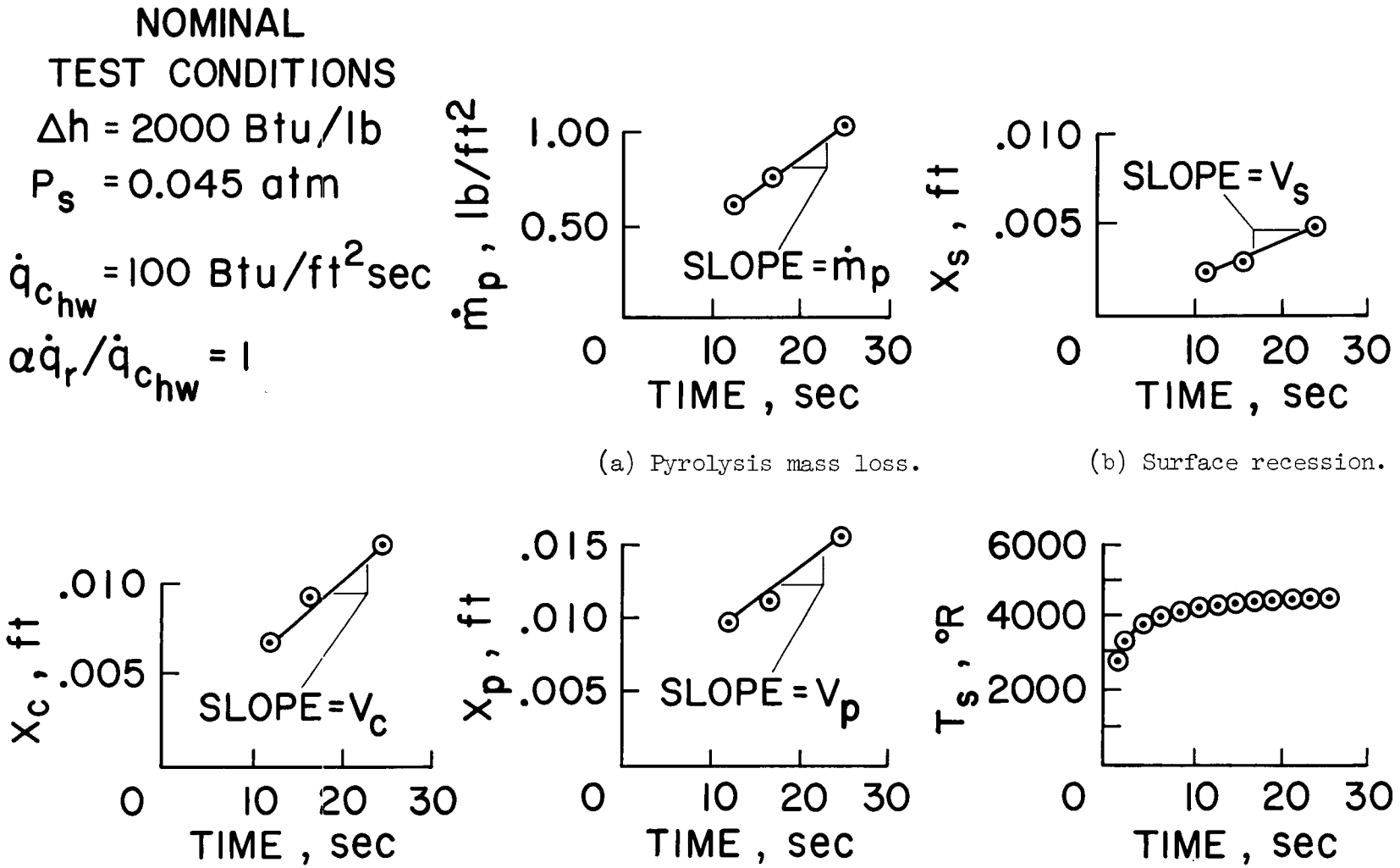

(a) Pyrolysis mass loss.

(b) Surface recession.

(c) Char interface recession.

(d) Pyrolysis interface recession.

(e) Time-temperature history.

Fig. 3.- Typical measurements.

NATIONAL AERONAUTICS AND SPACE ADMINISTRATION
AMES RESEARCH CENTER, MOFFETT FIELD, CALIFORNIA

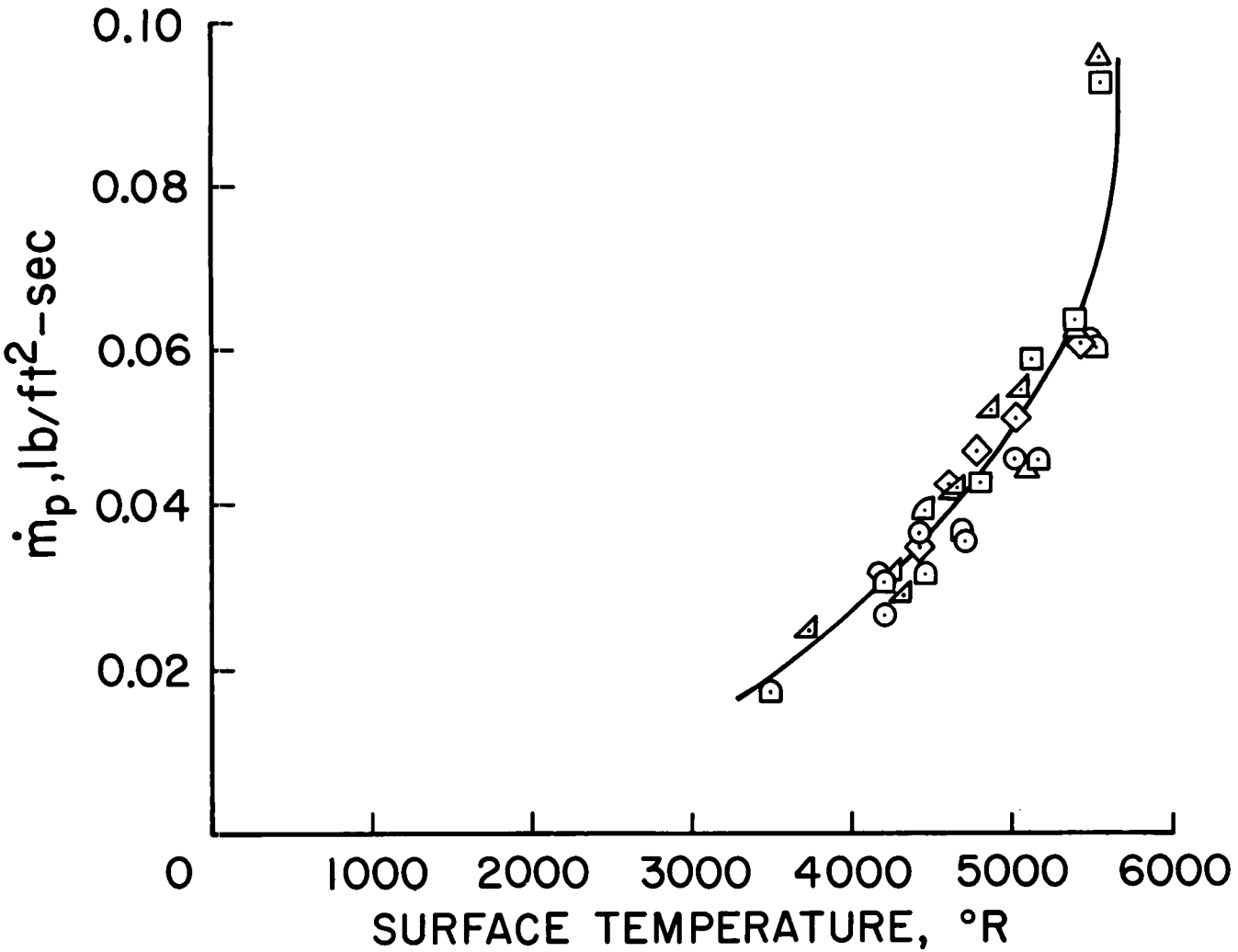

Fig. 4.- Pyrolysis rate.

NATIONAL AERONAUTICS AND SPACE ADMINISTRATION
AMES RESEARCH CENTER, MOFFETT FIELD, CALIFORNIA

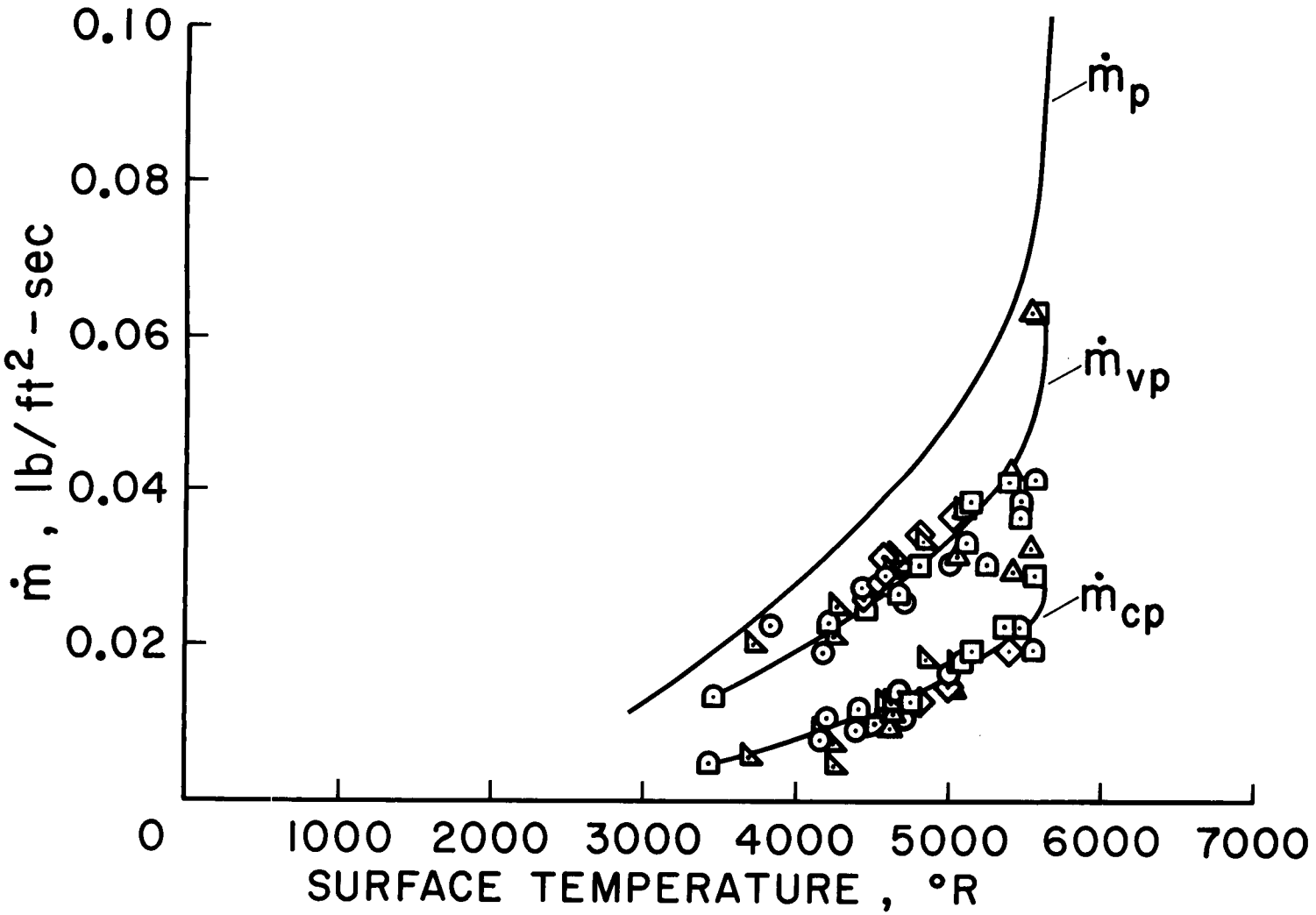

Fig. 5.- Production rates.

NATIONAL AERONAUTICS AND SPACE ADMINISTRATION
AMES RESEARCH CENTER, MOFFETT FIELD, CALIFORNIA

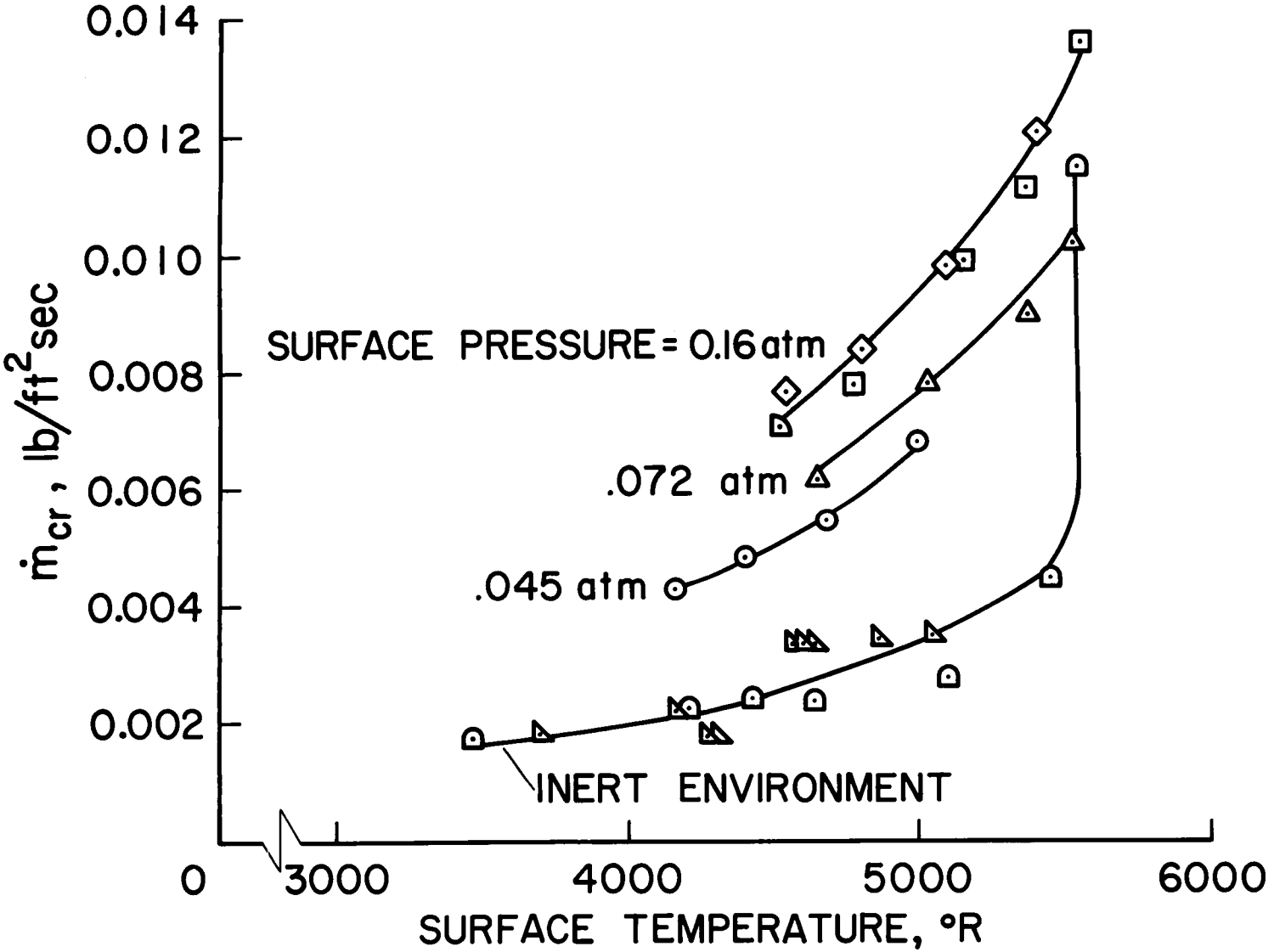

Fig. 6.- Char removal rate.

NATIONAL AERONAUTICS AND SPACE ADMINISTRATION
AMES RESEARCH CENTER, MOFFETT FIELD, CALIFORNIA

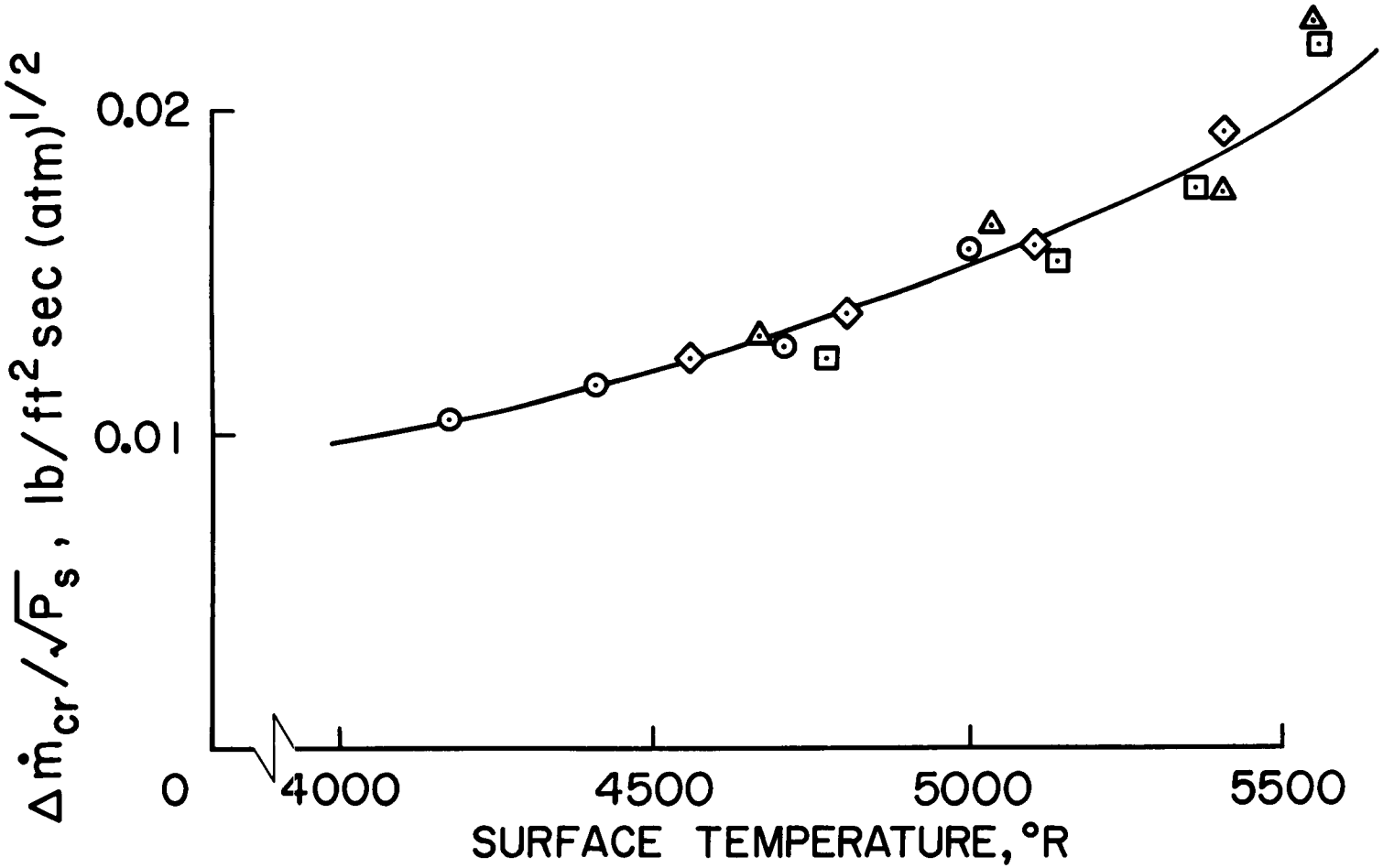

Fig. 7.- Char removal by surface combustion.

NATIONAL AERONAUTICS AND SPACE ADMINISTRATION
AMES RESEARCH CENTER, MOFFETT FIELD, CALIFORNIA

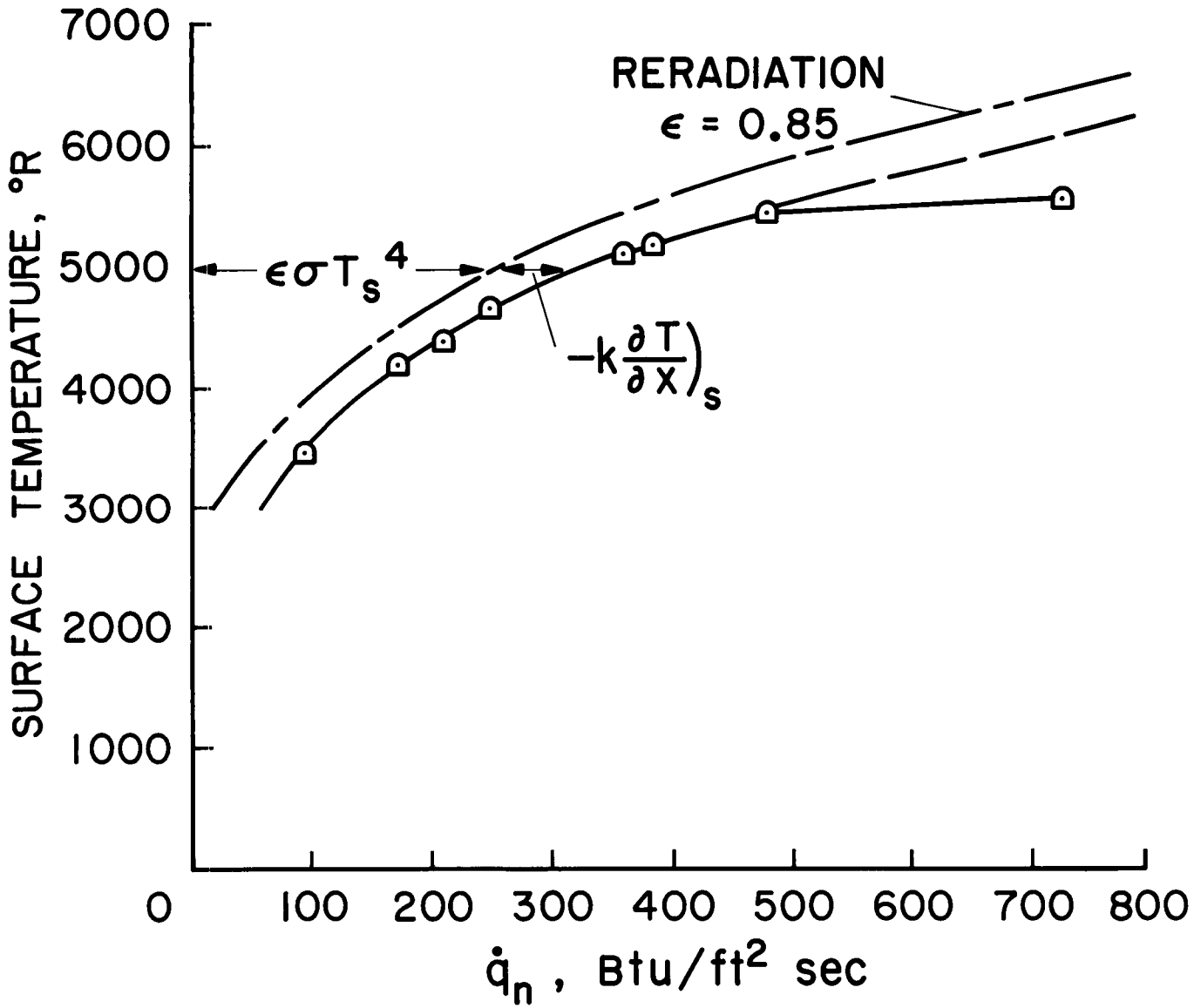

Fig. 8.- Net heating rate.

NATIONAL AERONAUTICS AND SPACE ADMINISTRATION
AMES RESEARCH CENTER, MOFFETT FIELD, CALIFORNIA

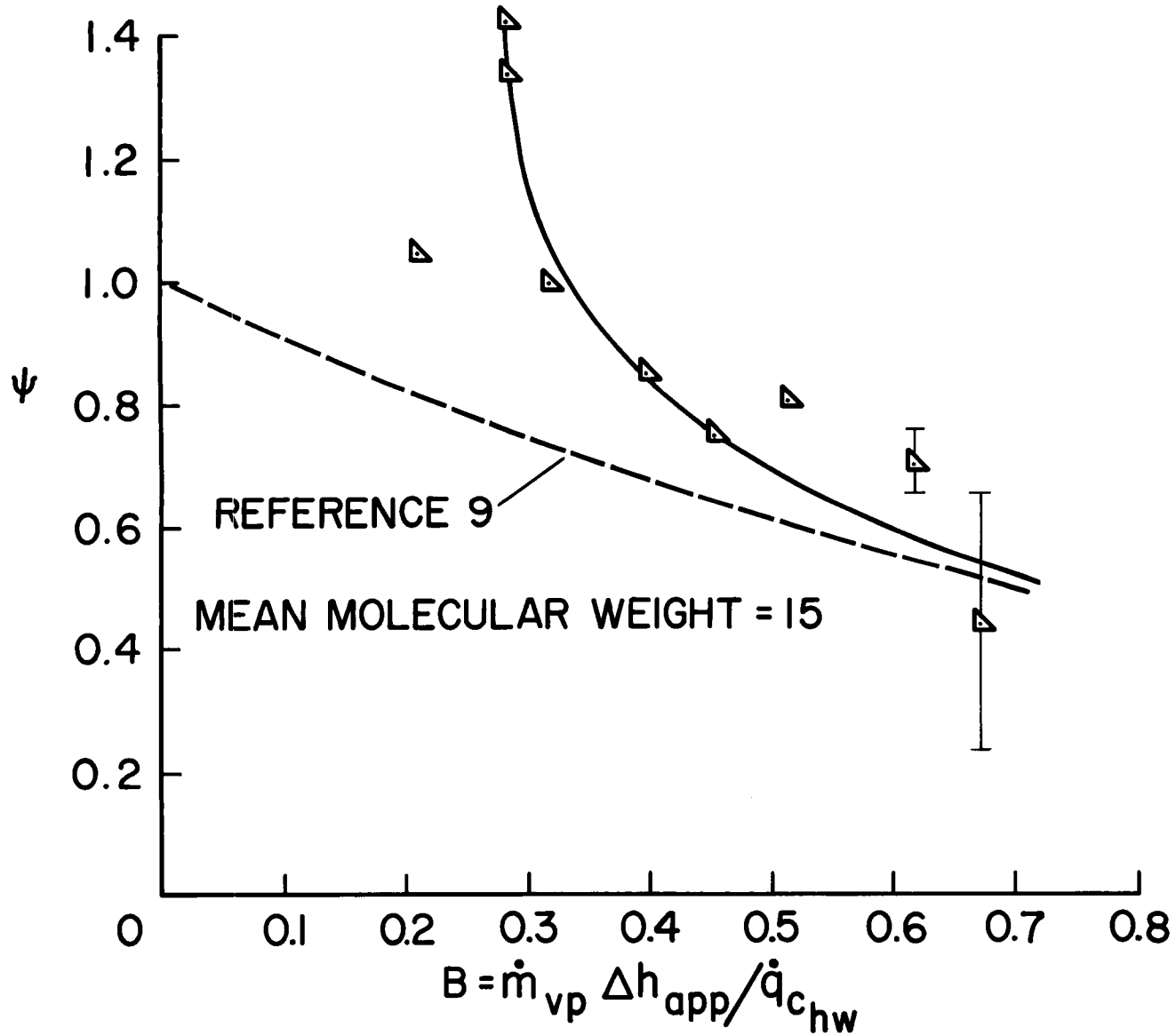

Fig. 9.- Convective blockage.

NATIONAL AERONAUTICS AND SPACE ADMINISTRATION
AMES RESEARCH CENTER, MOFFETT FIELD, CALIFORNIA

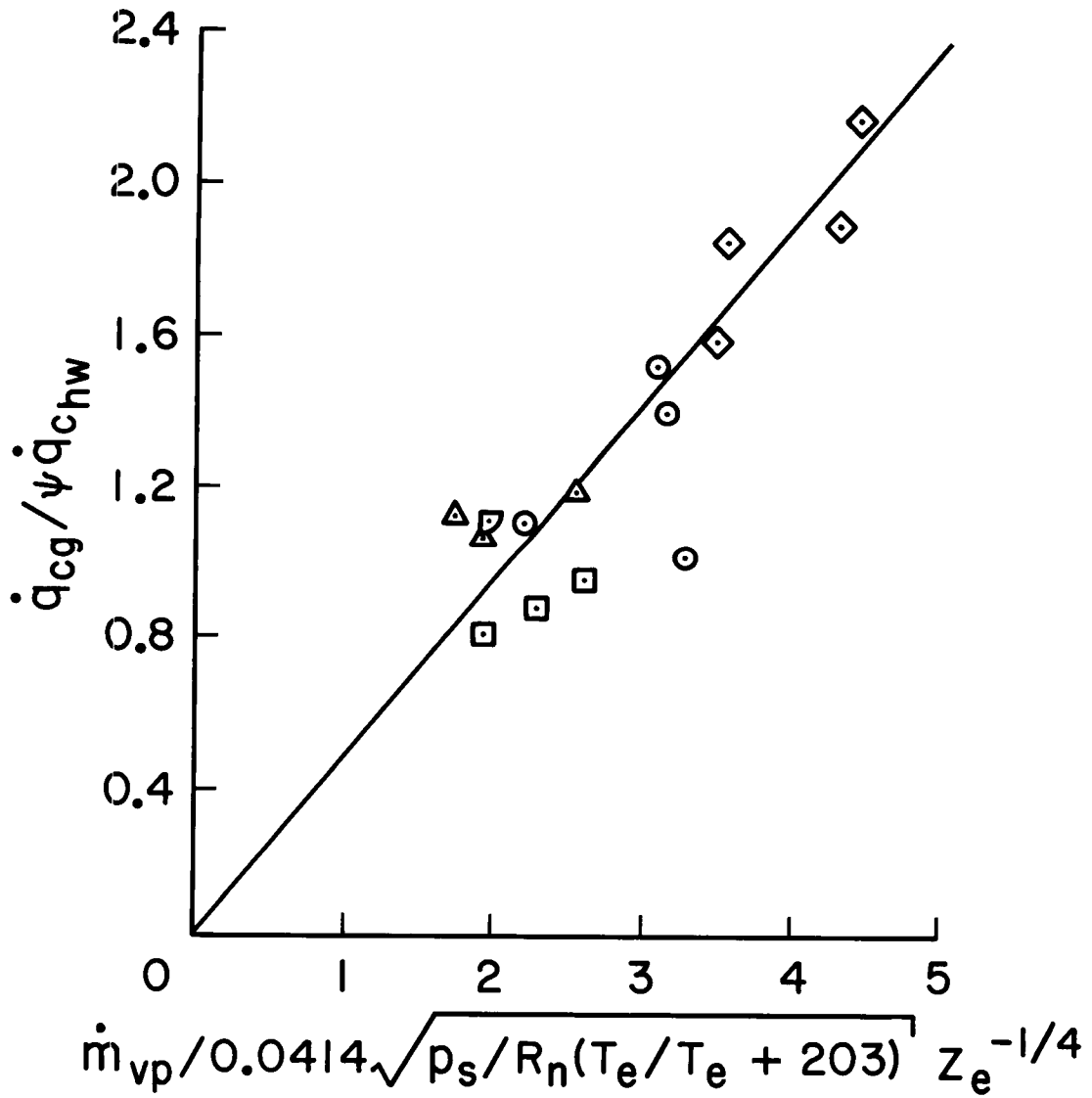

Fig. 10.- Gas-phase combustion.

NATIONAL AERONAUTICS AND SPACE ADMINISTRATION
AMES RESEARCH CENTER, MOFFETT FIELD, CALIFORNIA

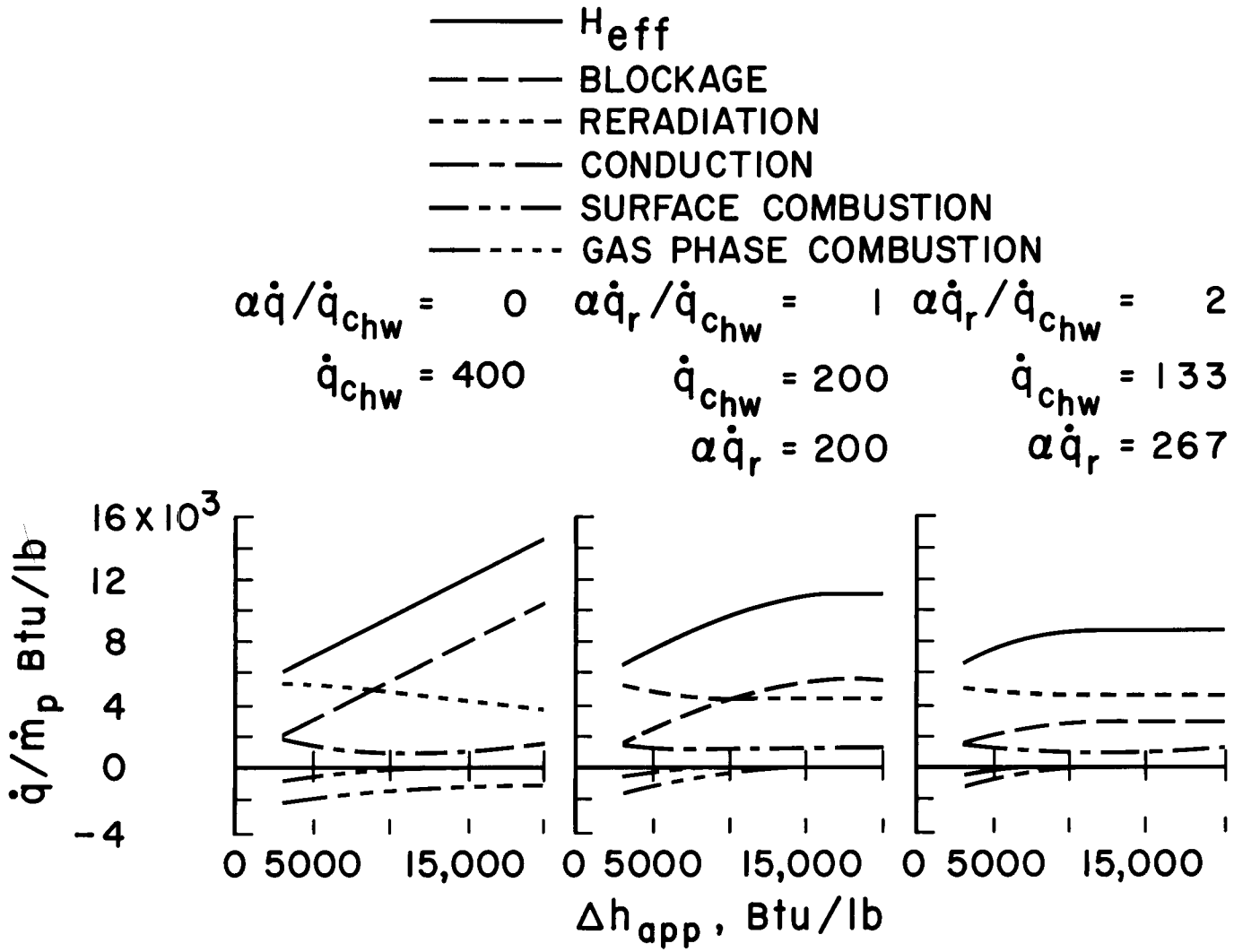

(a) Constant applied heating rate.

Fig. 11.- Components of H_{eff}.

NATIONAL AERONAUTICS AND SPACE ADMINISTRATION
AMES RESEARCH CENTER, MOFFETT FIELD, CALIFORNIA

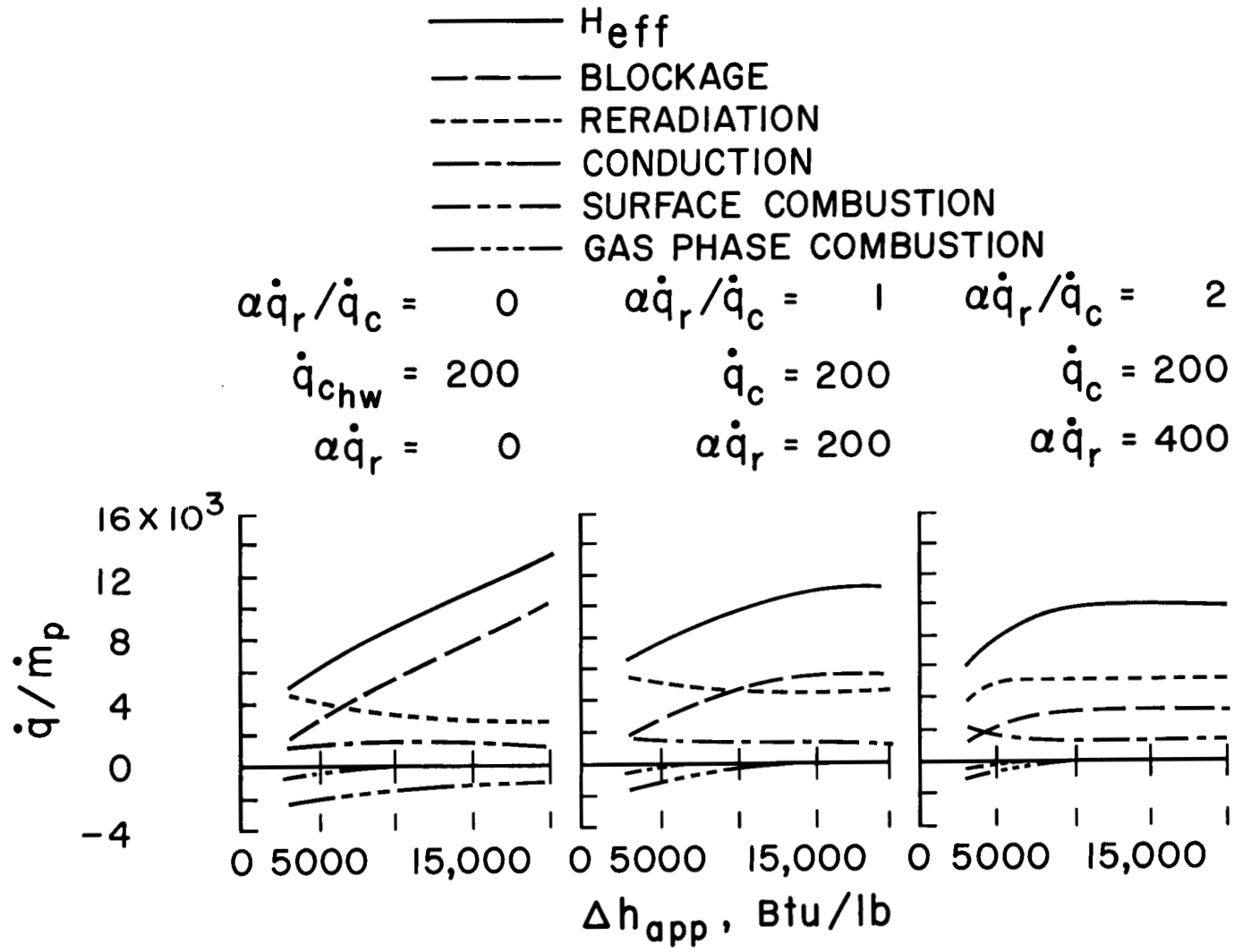

(b) Constant convective heating rate.

Fig. 11.- Concluded.

NATIONAL AERONAUTICS AND SPACE ADMINISTRATION
AMES RESEARCH CENTER, MOFFETT FIELD, CALIFORNIA

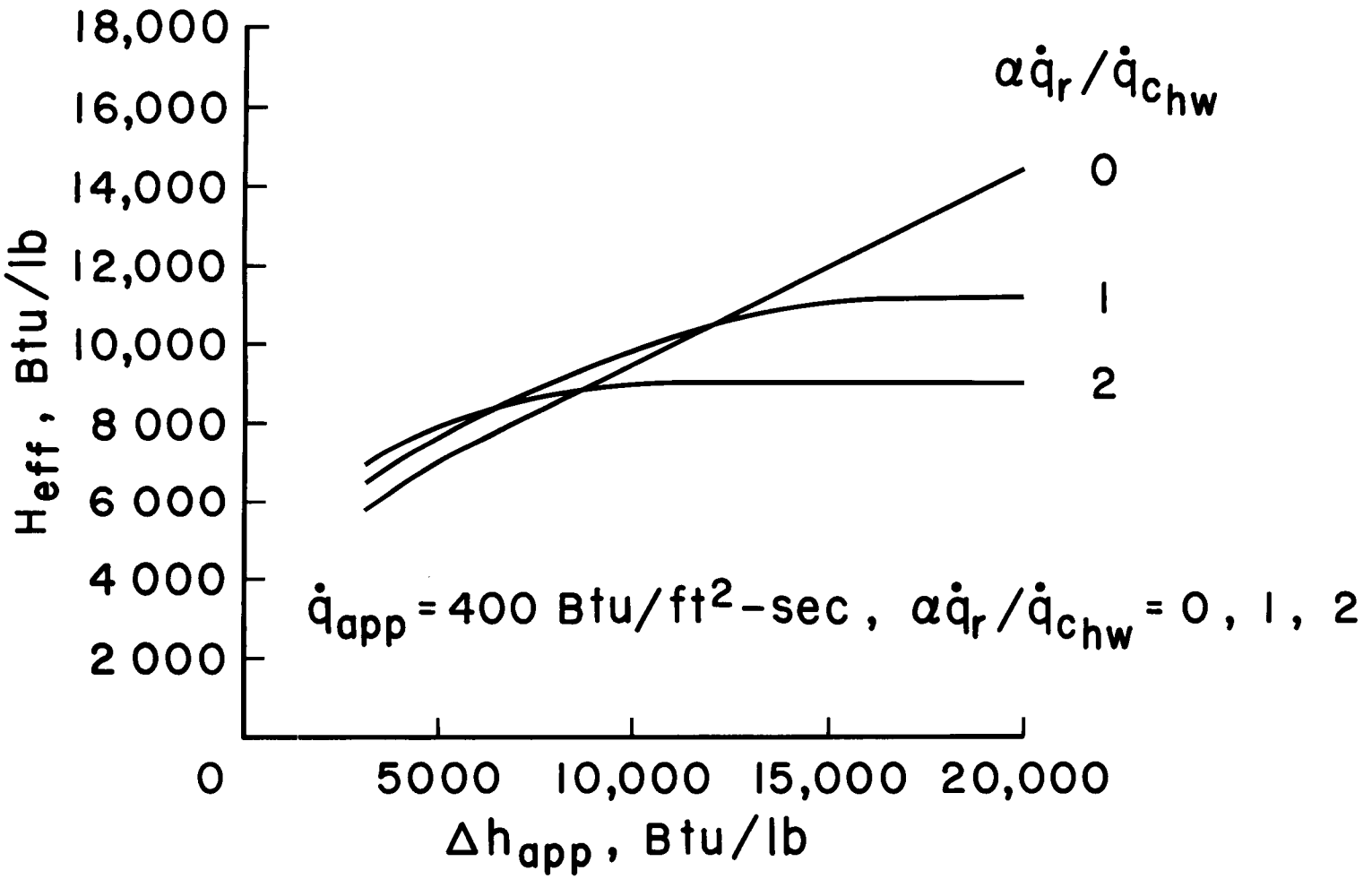

(a) Constant applied heating rate.

Fig. 12.- Effective heat of ablation.

NATIONAL AERONAUTICS AND SPACE ADMINISTRATION
AMES RESEARCH CENTER, MOFFETT FIELD, CALIFORNIA

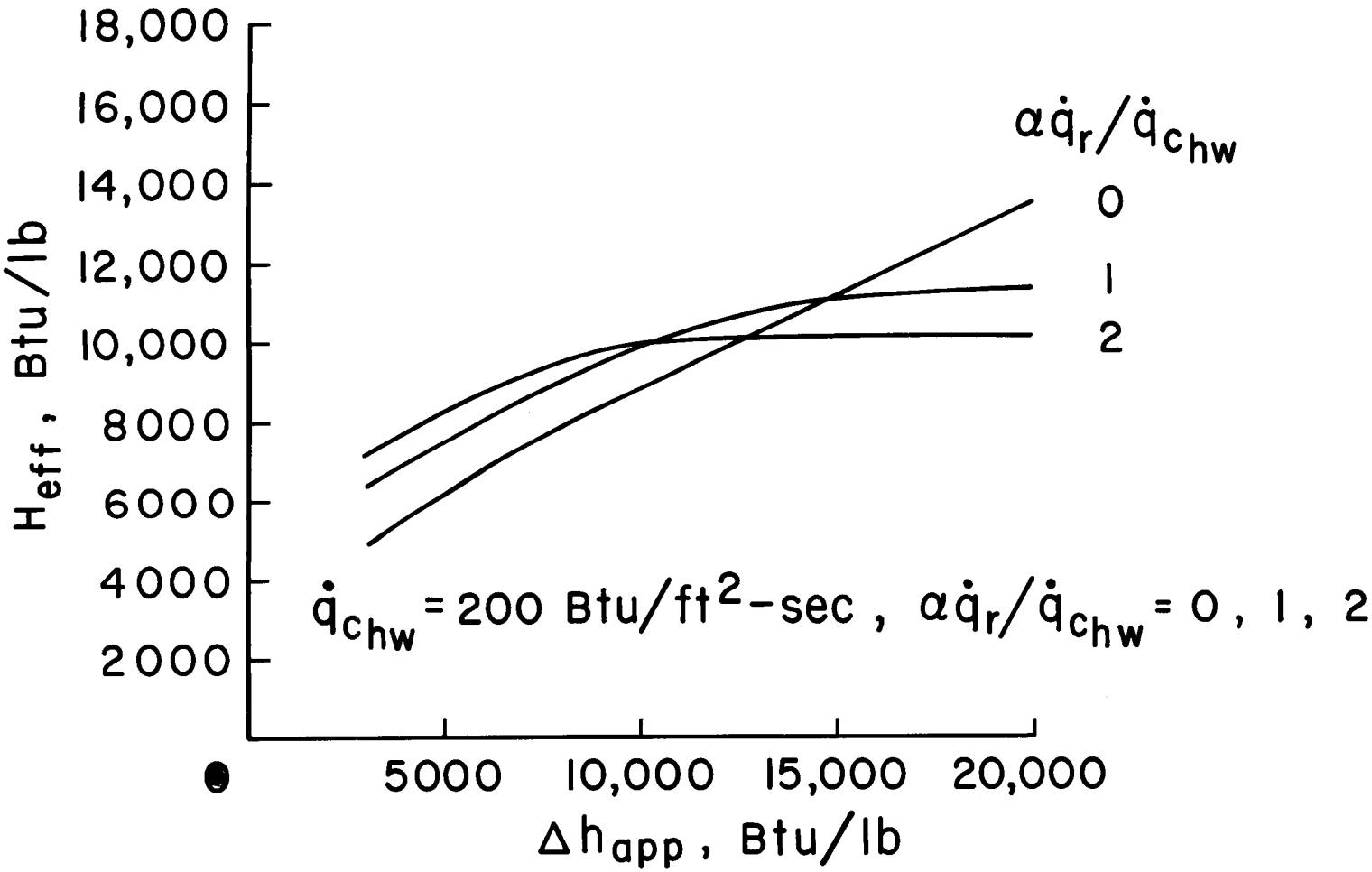

(b) Constant convective heating rate.

Fig. 12.- Concluded.

NATIONAL AERONAUTICS AND SPACE ADMINISTRATION
AMES RESEARCH CENTER, MOFFETT FIELD, CALIFORNIA